ΕΘΝΙΚΟ ΜΕΤΣΟΒΙΟ ΠΟΛΥΤΕΧΝΕΙΟ

ΔΙΑΤΜΗΜΑΤΙΚΟ

ΠΡΟΓΡΑΜΜΑ ΜΕΤΑΠΤΥΧΙΑΚΩΝ ΣΠΟΥΔΩΝ

«ΥΠΟΛΟΓΙΣΤΙΚΗ ΜΗΧΑΝΙΚΗ»

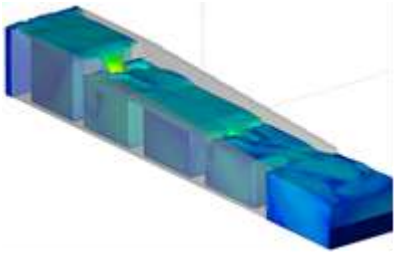

ΜΑΘΗΜΑΤΙΚΗ ΠΡΟΣΟΜΟΙΩΣΗ ΡΟΗΣ ΣΕ ΔΙΟΔΟΥΣ ΙΧΘΥΩΝ

Γεώργιος Β. Μητσόπουλος

Επιβλέπων: Α. Ι. Στάμου, Καθηγητής Ε.Μ.Π.

Αθήνα, Οκτώβριος 2016

NATIONAL TECHNICAL UNIVERSITY OF ATHENS

INTERDEPARTMENTAL PROGRAM OF POSTGRADUATE STUDIES IN
«COMPUTATIONAL MECHANICS»

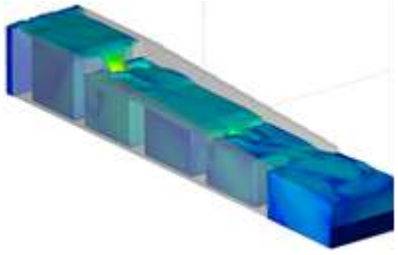

MATHEMATICAL MODELING
OF THE FLOW FIELD IN FISH-PASSES

Georgios B. Mitsopoulos

Supervisor: A. I. Stamou, Professor N.T.U.A.

Athens, October 2016

Table of Contents

Table of Figures

Table of Tables

Photos for the cover have been found at www.flow-3d.com and www.slideshare.net

ACKNOWLEDGEMENTS

This work has been carried out at the Department of Water Resources and Environmental Engineering of the School of Civil Engineering of the National Technical University of Athens (NTUA) under the supervision of Professor Anastasios I. Stamou.

I would like to express my gratitude to Professor Anastasios I. Stamou for the useful comments, remarks and engagement through the learning process of this master thesis. Furthermore, I would like to express my very great appreciation to Dr. Minh Duc Bui of Technical University of Munich (TUM) for his valuable and constructive suggestions during the planning and development of this work.

My special thanks are extended to Aleksandros Panagoulias and Georgia Papachristou, for their support and precious help.

I offer very special debt of deep gratitude to my family for their unceasing sacrifices and encouragement.

The present work was performed within the framework of a research project entitled "*Programme for the promotion of the exchange and scientific cooperation between Greece and Germany"*, IKYDA 2016. A part of this work was carried out in the TUM; Special thanks are also due to the DAAD, the TUM and the NTUA.

ABSTRACT

The prevention of fish migration, due to manmade technical works such as hydroelectric plants and dams, has severe environmental and ecological impacts on river and coastal ecosystems. Fish-passes are channels that create the right flow and environmental conditions to help fish migration either for reproduction or for food purposes.

The creation of fish-passes is highly complicated, because it depends on various fish characteristics. Therefore their design cannot relay on empirical observation and basic hydraulics. The prediction of the flow field, water depth and mainly the turbulent characteristics of the flow can be calculated from mathematical models with the use of computers.

In the present study a 3-D hydrodynamic model was employed. Using the commercial computer code FLOW-3D for flow calculation, the developed modeling approach provided good results of flow pattern. The mathematical model was based on Reynolds Averaged Navier Stokes equations with a closure model for the Reynolds Stresses Tensor, the Renormalised Group k-epsilon.

This methodology was applied on an experimental fish-pass and the results were compared with the experimental measurements. Moreover the model created was compared to a 2-D numerical simulation, which solved the shallow water equations with the use of the standard k-epsilon turbulent model.

Keywords: Fish-pass, RNG k-ε Turbulent model, FLOW-3D, Vertical Slot.

Περίληψη

Η παρεμπόδιση του ταξιδιού των μεταναστευτικών ψαριών, λόγω ανθρωπογενών τεχνικών έργων, όπως τα μικρά υδροηλεκτρικά και φράγματα, έχει σοβαρές περιβαλλοντικές και οικολογικές επιπτώσεις στα ποτάμια και παράκτια οικοσυστήματα. Για να βοηθηθεί και να υποστηριχτεί η μετανάστευση των ψαριών, είναι απαραίτητη η δημιουργία διόδων ιχθύων. Οι δίοδοι ιχθύων είναι κανάλια, που είτε προσομοιάζουν τα φυσικά είτε όχι, δημιουργούν τις κατάλληλες ροϊκές και περιβαλλοντικές συνθήκες για να βοηθηθούν τα ψάρια που μεταναστεύουν είτε για αναπαραγωγή ή για τροφή.

Η δημιουργία των διόδων ιχθύων είναι ιδιαίτερα περίπλοκη, επειδή εξαρτάται από τη συμπεριφορά των ψαριών, τα κίνητρα, τις προτιμήσεις, το χρονοδιάγραμμα της μετανάστευσης και την ικανότητα κολύμβησης. Αρχικά οι μηχανικοί προσπάθησαν να δημιουργήσουν τα περάσματα ψαριών με βάση την εμπειρική παρατήρηση και τη βασική υδραυλική. Σήμερα, που η υπολογιστική ισχύς εξελίσσεται ραγδαία, πολλά μαθηματικά μοντέλα έχουν αναπτυχθεί για να περιγράψουν τη συμπεριφορά και να προβλέψουν το πεδίο ροής, το βάθος του νερού και κυρίως τα τυρβώδη χαρακτηριστικά της ροής μέσα σε μια δίοδο ιχθύων.

Στην παρούσα μελέτη, ένα υδροδυναμικό μοντέλο, που βασίζεται στις σταθμισμένες κατά Reynolds εξισώσεις Navier – Stokes, χρησιμοποιήθηκε για τον υπολογισμό των χαρακτηριστικών ροής. Ως μοντέλο για τον υπολογισμό του τανυστή των τάσεων Reynolds, χρησιμοποιήθηκε το μοντέλο k-έψιλον Renormalised Group, το οποίο βασίζεται στην υπόθεση του Boussinesque, περί τυρβώδους συνεκτικότητας.

Αυτή η μεθοδολογία εφαρμόστηκε σε πειραματική δίοδο ιχθύων και τα αποτελέσματα συγκρίθηκαν με τις πειραματικές μετρήσεις. Επιπλέον το μοντέλο που δημιουργήθηκε συγκρίθηκε με αριθμητική προσομοίωση με τη χρήση των εξισώσεων shallow water και χρήση του k-ε μοντέλου τύρβης.

Τέλος για την σύγκριση των 2 μοντέλων δημιουργήθηκαν 3 προγράμματα σε γλώσσα προγραμματισμού Visual Basic Excel και C#, ώστε να υπολογιστούν οι κατάλληλοι δείκτες και να βρεθούν τα μέσα μεγέθη της ροής.

Chapter 1. Introduction

An important environmental problem, which is created from man-made mostly technical works, is the prevention of migration of fish, like salmons and trout, move from upstream to downstream and the opposite. The main problem is created in rivers, lakes or streams, where artificial or natural barriers, such as dams, locks and waterfalls, exist.

Fish migration is a cycle of upstream and downstream movements. The type of movement depends on the fish's life stage, its location, and the type of migration. When downstream migration is mentioned the fish are at an early life stage, while upstream migration refers to adult life. Spawn, feeding and seeking refuge from predators or harmful environmental conditions are the main reason for migration.

The solution is the creation of waterway structures, called fish-passes, to help the migratory fish from the downstream side of the obstacle to the upstream. Most of them are being created to help the spawning of adult migratory fish, something that is critical for the continuity of the species in the specific environment. Furthermore fish-passes are created to support the migration of juvenile fish in search of food and better conditions.

The first written reports of fish-passes are dated back to 17th-century France (McDonald 1887; Rajaratnam and Katopodis 1984), where bundles of branches were used to create steps in steep channels to bypass obstructions. A Canadian, Richard McFarlan, was the first to design a fish-pass in 1837 for his own windmill. In 1852–1854, the Ballisodare Fish-pass was built in County Sligo in Ireland to draw salmon into a river that had not supported a fishery. In 1880, the first fish ladder was built in Rhode Island, United States, on the Pawtuxet Falls Dam.

Fish-passages require an adequate design and construction in terms of safety and adequate provision to maintain healthy fish populations. Well designed and constructed fish-passes provide a waterway that allows fish migration without unacceptable delays. Biological requirements such as fish behavior, motivation, preferences, migration timing and swimming ability drive design and construction criteria for fish-passes (Katopodis 1992). Although some requirements such as migration timing and the corresponding hydrological conditions in rivers and streams, or swimming performance and fish-passes hydraulics can be harmonized through rational approaches, other requirements such as species preferences, motivation and behavior rely heavily on experience and judgment.

Swimming ability is a key component in the successful completion of fish migrations. Fish upstream movement deals with a variety of flows, water velocities and depths. This range from areas of slow currents, such as pools, wide river sections or reaches of mild stream gradients, to areas of fast currents, such as rapids, narrow sections or reaches with steep gradients. Fish are capable of overcoming such difficulties by using different levels of swimming performance. This performance has been classified into burst speed (highest speed attainable and maintained for less than 15 seconds), prolonged speed (a moderate speed that can be maintained for up to 200minutes), and sustained speed (a speed maintained indefinitely) (Katopodis 1992). In natural fish-passes sustained and prolonged speeds are used more often and occasionally burst speeds in order to overcome high velocity areas.

As mentioned above fish-passes allow fish to a) maintain migrations through technical works, b) re-establish migrations after years of blockage at man-made barriers, or c) extend migrations upstream of natural barriers. But in order to be functional must provide safety and effective route in an acceptable time frame.

Safety through a fish-pass means that the diadromous fish will pass through with minimal injury or mortality resulting from the project barrier or impediment. Ideally, the safe passage objective is 100% survival, although it is not always the case. Adequate time frame has been described as minimal delay of migration movements past the barrier to the extent needed to achieve restoration goals. Excessive delay of passage can result in adverse effects on reproductive potential through many factors. Site and project operational considerations and target species should be considered in order to promote the best achievable passage. Finally effectiveness is achieved when most if not all diadromous fish arriving at the barrier successfully pass to upstream/downstream habitats without impact on their natural biological functions. Ideally, 100% of the individuals of the target species would be passed. However, as with rates of safe passage, project-specific objectives will reflect the details of restoration goals, site conditions, and project operation limits (National Marine Fisheries Service, USA 2009).

In order all the above to be achieved, the correct design of a fish-pass demands presence or absence of target fish species, fish behavior and timing of migration peaks, fish physiology and biomechanics, hydraulic analysis, and mechanical and structural engineering design concepts compatible with the physical characteristics of the barrier or dam. In some cases, installation of fish-passage was not viable because of adverse habitat quality above a dam, total absence of former natural spawning runs, or significant threats imposed by harmful exotic and invasive species potentially passed upstream or downstream to adversely affect river ecology. It is

important to mention that in most cases, if a burrier or technical work is no longer functional, it is for the best to be removed and return the site to its former condition.

1.1 Fish-Pass Type

Fish-passes consist of a sloping channel partitioned by weirs, baffles, or vanes with openings for fish to swim through. In these hydraulic devices the fish can navigate easily. Several types of fish-passes have been proposed and used and have many similarities. The main though and most used are the pool passes, the Denil passes and the vertical slot.

Figure 1 Example of vertical slot fish-pass with guiding walls

Source: www.fao.org

1.1.1 Denil Fish-pass

A Denil fish-pass is another design of fish-way, which consists of a channel with closely spaced baffles or vanes located along the sides and bottom. It took the name after the Belgian engineer, Denil, who invented it. The Denil contains a series of concave-shaped baffles pointing upstream, at an angle of 45 degrees with the fish-way floor. Today the concave baffles have been almost completely replaced by u-shaped ones with triangular bottom.

Flow through Denil fish-passes is highly turbulent, with large momentum exchange and high energy dissipation. The water in the chute flows at a relatively low velocity near the bottom with a faster velocity near the top. At high depths, flow divides into an upper and a lower layer, and velocity profiles become roughly symmetrical with

maximum velocities at mid-depth. The advantages of the Denil fish-pass is that because it is functional with high bottom slopes, they can be used in already existing technical works, when space is limited. Generally it is proven from the already constructed fish-passes that this design is easily spotted from the fish and itis not susceptible to the flow depth level of tailwater.

On the other hand the disadvantages are that the variations of headwater level play a significant role to the functionality of the fish-pass. Only few cm variations are allowed. Moreover is not functional in low discharges and it needs frequent cleaning.

By monitoring existing installations it is noticed that although Denil fish-pass are adequate for big salmonoids, its efficiency is highly limited for smaller fish. Likewise, ascent by microorganisms and invertebrate benthic fauna must be rated impossible.

Figure 2 Denil fish-pass

Source:www.kleinschmidtgroup.com

1.1.2 Pool Fish-passes

The Pool Fish-passes consist of a channel divided by a number of pools arranged in a stepped pattern separated by baffles. The fish movement between the pools usually demands burst speeds, but also the pools provide resting areas.

Pool fish-passes have 4 main variations, which were created at the process of development. These variations are:

1.1.2.1 The weir fish-pass with cross walls vertical to the channel

In weir fish-passes baffles are of rectangular shape and each of which is constructed higher the next downstream one and vertical to the ground and to the flow.

The fish, attracted by the flowing water, move from pool to pool by jumping or swimming (depending on the water depth) until they have cleared the obstruction. Usually they have also a hole at the submerged part and a cut at the upper part, to help fish-pass through the holes in case they are not able to jump above the weir. They are simple to construct, they manage to dissipate the discharge in fish swimming potential levels and create high velocity currents only near the wall, while in general the velocity field is kept low. The main disadvantage is that the pool and weir is sensitive to fluctuating water levels and requires frequent adjustments. The water level drop between pools is usually set at 30cm for adult salmon and 20 cm for adult freshwater fish. Weir fish-passes usually have a slope of10%. The dimension must be selected based on the dissipation of the discharge needed by the fish that are going to use the pass. Sometimes the baffles go underwater and that creates negative effects to the flow making the fish-pass not desirable for fish to use.

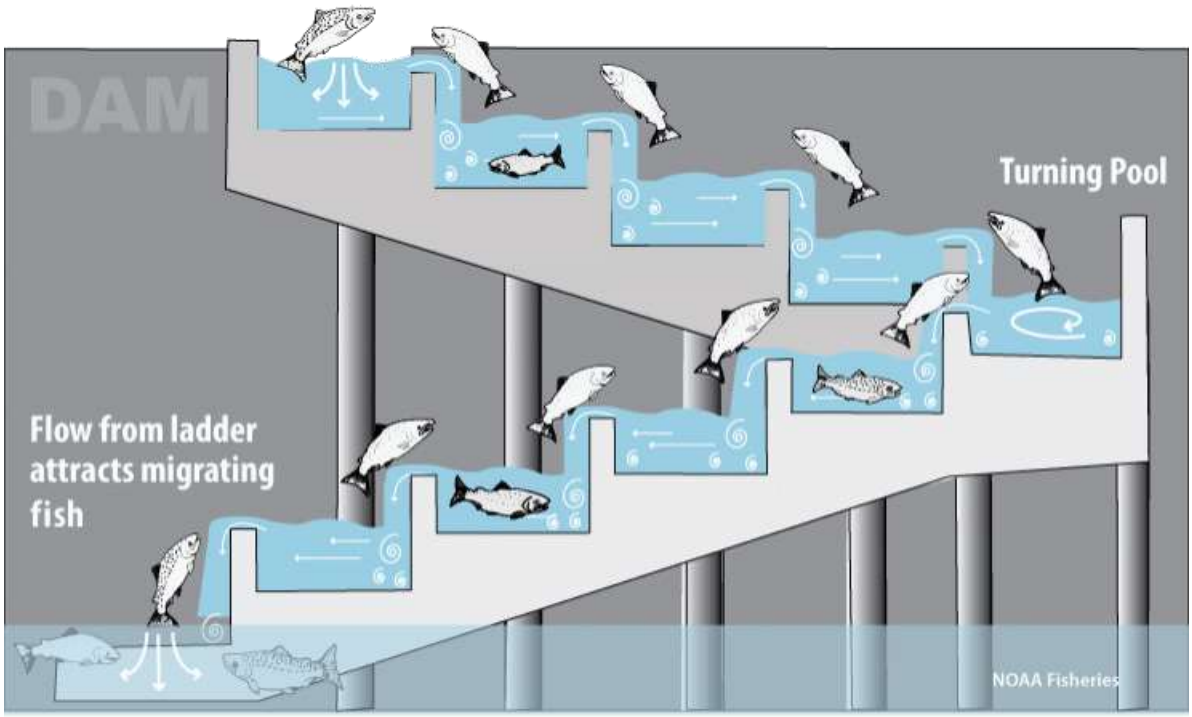

Figure 3 Weir Fish-Pass

Source: www.civilgeo.com

1.1.2.2 The rhomboid cross wall weir fish-pass

The only difference in this variation of the weir fish-pass is the fact that the baffles have a rhomboid shape. They are usually constructed at an angle to the channel walls with the upstream upper part submerged and the downstream having the notch. The advantages in comparison to the first category are the improved flow characteristics, with lower velocities and slightly less turbulence, the direction of the flow which helps fish orientation and the easier cleaning.

The humped fish-pass

Special form of the pool pass in which the orifices are designed as widening streamline channels (Henson & Schiemenz, 1960). The general criteria apply here also. The advantage is that the orifices are not parallel to one another, but aligned which does not create eddies and rollers vortexes in the pools. On the other hand they need too much space and work only in small pool depth differences.

Figure 4 Pool fish-passes (a) with orifices at the center of the wall and (b) with weirs

Source: www.slideshare.net

Figure 5 Rhomboid pool fish-pass

Source:http://www.fao.org/docrep/010/y4454e/y4454e00.HTML

1.1.3 Culvert Fish-Passes

Culverts are channels that are used to let water pass underneath construction such as roads. Culverts are built with circular, elliptic, pipe-arch, rectangular or square cross-sections. When a culvert is used it must be ensured that the fish will be able to pass unharmed and without delay. In many cases culverts are placed below the stream bed. They are mainly used at roadway construction with slopes of 0.5 and 5%.

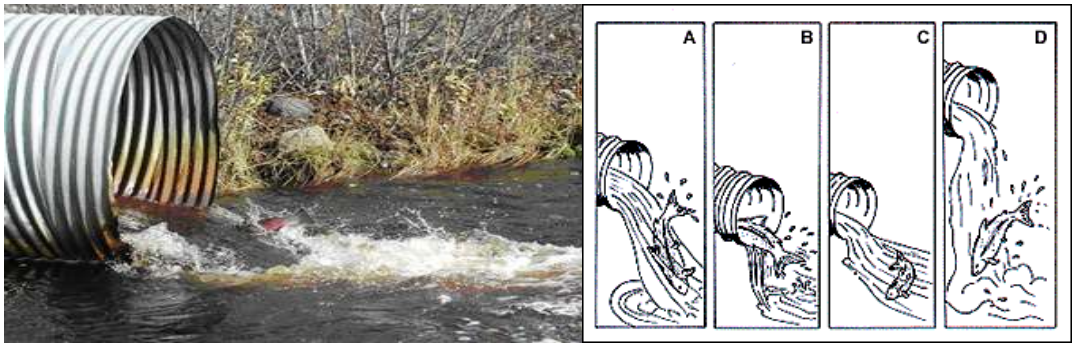

Figure 6 Examples of culvert fish-passes and their use

Source: www.adfg.alaska.gov&www.na.fs.fed.us

1.1.4 Lift Fish-pass

In case of significant height difference (> 6 to 10 m) and little water available , the use of the above mentioned fish-passes is not an option, due to the building costs, the space requirement and the overall depiction on the fish. A solution proposed to overcome such problems is by using a lift. A trough is used as a lift. When in the lower position, the trough is sunk into the bottom. Fish are pushed towards the lift by a guide current. Moreover a sliding and collapsible grid gate located in front of the lift, may serve to push the fish into the trough. The lower gate of the lift closes and he fish trapped in the trough are conveyed to the top. Along with the water also trapped in the trough, the fish with the help of a current are left to the headwater. The repeated cycle is based on the migration needs of the fish.

Although the lift solves the problem of height and space and it can move migratory fish upstream without exceptions, the expenditure for maintenance and the construction cost are high and the variations of tailwater levels must be taken seriously under consideration. Finally lifts are suitable for migration from downstream to upstream and not the other way around.

Figure 7 Fish elevator

Source: www.winwes.com

1.1.5 Vertical Slot Fish-passes

A vertical slot fish-pass can be a part of the pool fish-passes. It consists of a sloping channel partitioned from baffles into pools. The difference is that the baffles have a vertical slot, which extends over the entire height of the baffle. There can also be a second slot depending on the needs of the fish-way. The slots are always offset one another. An advantage is that the fish can easily maintain their course within each pool. However the velocities of the water vain in the slot require a burst effort from the fish to pass through the slot, while traveling upstream. Water velocities whatsoever at the slots remain almost the same through the entire height of the slot. With the use of a vertical slot fish-way large variations in water level scan be handled. Usually the difference between water levels in successive pools is 30 cm for salmon and 20 cm for adult freshwater fish. Vertical slot fish-passes usually have a slope of 5% to 10%. Generally the fish-pass with some additions (bottom substrates) are suitable for most of fish species and fish sizes. Also because it is used extensively that's why is the fish-pass that is going to be studied in this dissertation.

Figure 8 Vertical slot fish-passes (a) with two slots and guiding baffles (b) with one slot without guiding baffles

Source: http://www.fao.org/docrep/010/y4454e/y4454e00.HTML

Chapter 2. Literature review

As mentioned above the vertical-slot fish-passes are the most commonly used, because of their flow characteristics, which support most types of fish. For this reason they have been expensively studied, both through experiments and numerical simulations.

The experimental studies started at late 60. But the in depth experimental study was made by Rajaratnam et al.(1986). They studied 7 different designs for different scale models 1:1, 1:5.33, 1:8, and 1:16. The dimensions of the pools were proportional to the width of the slot b_o, specifically the length was 10 times b_o and the width 8 times b_o.

In all the designs they studied the mean flow structure in the pools. They assumed an idealized uniform flow, where the mean flow depth is the same. This was mainly supported from the experimental observations. Through the experiment the fluid friction coefficient C_f was mainly steady, who indicates a linear relation between the dimensionless discharge $Q/\sqrt{(gSb^5)}$ and the relative flow depth y_o/b_o, where Q is the discharge, g is the gravity acceleration, S is the bed slope, b is the slot width and y_o the water depth at the center of the pool.

With the 1:5.33 scale model and different tail water levels a large amount of velocity profiles were obtained both 2-D and 3-D. For most of the profiles the jet velocities are uniform, with a small decrease near the water surface. When the tail water depth is low, the jet velocity at the final slot, near the tail water is excessive. In general the maximum velocity at any slot was close to$Vmax = \sqrt{(2gdh)}$. Finally through the circulation measurements, they conclude that the flow is 3-dimensional and the jet path vary according to the tail water level and the discharge. The energy of the jet is dissipated, which creates recirculation areas above and below the jet vain.

Rajaratnam et al. 1992 conducted an experiment with 18 different designs of vertical slot fish-passes. They studied the relation between the width and length of the pools with the slot width. They concluded that a relation between widths W is $8b_o$ and length is $10b_o$.Minor variation of these relations does not change the performance of the fish-pass. But low widths tend not to dissipate the jet energy and create strong circulation The linear relation between the dimensionless discharge and he relative depth was confirmed for also the rest of the designs. To measure the energy dissipation in the pools, the dissipation rate k was calculated. The relation between k and the relative depth y_o/b_o shows that each design has a different rate and also that

slope plays an important part. The discharge coefficient was found to be not adequate on its own to judge the performance of a vertical slot fish-pass. In contrast to that the friction coefficient remains the same for all the designs. Finally a recommendation for designs 6, 16, and 18 for practical use, based on overall performance and simplicity in design and construction was given.

Wu et al. (1999) made a laboratory experiment on vertical fish-passes using design 18 with a model scale of 1:2.67 for three slopes of 5, 10, and 20% with several discharges. They observed two typical flow patterns in the pools. The first pattern named was observed only in slope of 5% with several discharges and the trajectory of the jet was from one slot to the next through the center of the pool with two recirculation regions located on either side of the jet. The water level was almost horizontal, the flow was uniform and 2-dimensional and the recirculation volume in the pool was reaching 78%.

The second pattern was mainly observed in slopes 10% and 20%. the jet traveled towards the side wall in between the long baffles with a recirculation region created between the short baffles along with a horizontal eddy near the long baffle on the downstream end of the pool. In this case the water surface was not horizontal but was rising close to the downstream long baffle. For steep slopes and low discharge a hydraulic jump was observed together with dry spaces, the flow was non-uniform and thus 3-dimensional and the recirculation volume in the pool was reaching 38%.

The jet flow was studied through theoretical vertical planes in the general direction of the jet instead of along the jet trajectory. The result was that the velocities were not perpendicular to the slot and were non-uniform. Because of this the flow from the slot can be roughly only approximated with plane jet. Moreover is rapidly decreasing away from the slot, which results to the rapid decreases of the energy dissipation. This makes the fish-pass desirable for the fish. Finally they observed that in the first pattern the maximum slot velocity occurred near the surface and in the second pattern near the bed. Also the maximum velocity of the pool was not found at the slot but at a distance equal to b_o away from the slot at the direction of the flow.

Puertas et al.(2004) conducted an experiment regarding the vertical sot fish-pass designs 6 and 16 of Rajaratnam et al. 1992 here T2 and T1 respectively. They used 2 different slopes 5% and 10% and measured velocities with a microacoustic Doppler velocimeter microADV, in order to be able to measure it 3 dimensionally. They also followed the uniform hypothesis of Rajaratnam et al. 1992 and found the linear relation between the dimensionless discharge and the relative flow depth. The

maximum flow depth appears upstream just before the slot and downstream near the large baffle wall and the minimum after the slot, because we have a rapid water drop at the direction of the jet. The water surface was found to be independent of discharge. Regarding velocity fields and flow patterns, they also found that the jet creates a main flow area and two recirculation areas, one between the large baffles and a smaller between the short baffles. The size of the eddies was found to be in relations with the discharge, which above a certain value in design T1 create a second smaller eddy at the downstream large baffle. The z coordinate of the velocity field was found to be almost everywhere near zero, which leads to bidimensionality of the flow. Lastly the turbulent kinetic energy was found to be in straight relation only with the slope and the baffle dimensions. There is little dependency between the kinetic energy and the distance from bed, with the exception of high turbulence zones near the water surface.

Although all the previous experiments dealt with the velocity fields the relation of discharge and depth and the recirculation patterns, the turbulence characteristics study was limited and only a rough approach could be presented. Liu et al.(2006) used a microADV to study the turbulent characteristics of the flow in a vertical fish-pass, using the same design as Wu et al.(1999), design 18 of Rajaratnam et al. 1992.They conducted 2 experiments one for the turbulence characteristics and mean structures of the flow and one focused on the jet and its trajectory. They conducted the experiment for 2 different slopes 5.06% and 10.52% and 2 discharges 31.2 l/s and 52 l/s. They confirmed the results from Wu et al. (1999) and concluded that the flow from the slot can be described from a plane jet, although the longitudinal velocity decays rapidly. Moreover the turbulent jet cannot describe the turbulent structures of the flow, but it has some similarity, especially the dissipation rate. Those results were also confirmed by the Tarrade et al. (2011), who also studied the turbulence structures in vertical slot fish-passes. They used a form of design 16 of Rajaratnam et al. (1992). Through their experiment they concluded that the slope influences the turbulent characteristics and the mean velocity. Also they found that discharge does not affect the flow, but the water depth. Finally they reached the conclusion that only a part of flow characteristics can be approached by mean behavior.

Because of the difficulties that occur in making an experiment for fish-passes, such as cost, time and space, CFD is an alternative, which can help evolve our knowledge

on the flow characteristics. Thus lots of investigators studied the vertical slot fish-passes through CFD.

One of the first attempts to verify experimental results with CFD was calculations made by Barton et al.(2003). They used a commercial code ANSYS FLUENT to verify a CFD model based on the experiments made by Wu et al. (1999). They constructed the exact model that Wu et al (1999) had created in the lab. They used the 52 l/s discharge and they solved the Reynolds Averaged Navier Stokes equations, with the use of RNG κ-ε model for closing the turbulent model. To calculate the water surface, the Volume of Fluid method was used. The boundary conditions were the desired flow rate at the inlet and hydrostatic pressure with surface elevation at the outlet. Roughness coefficients were taken into consideration, but they had little influence to the result. The mesh used was unstructured quadrilateral/hexahedral with adaptations to accurately resolve the flow equations. The results are for the velocity field and the water depth show good comparison. There is a tendency of overestimating or underestimating the values close to the bed surface and the water surface, but it can be minimized with good grid adaptation. Moreover the water surface produced from the code adapts well to the experimental data, although there is an overestimation near the slot, which may occur due to accuracy problems. Finally the turbulence analysis can give a good estimation of what occurs in the pools, although there is no sufficient experimental data and the turbulence models has low accuracy because of the mesh.

Fujihara et al. (2003) made also an attempt to apply a numerical model on vertical slot fish-passes. They observed that by that time few numerical models had been applied, since the flow is really complex and their approach was not based on experimental mean flow models. They used the shallow water equations, which are solved with an approximate Riemann solver, through a Runge-Kutta scheme. They modeled three single slot designs and one double slot, similar to design 16 from Rajaratnam et al.(1986). The first attempt was a double slot vertical fish-pass. They resulted at a flow pattern almost the same with various water depths. The flow found sub-critical except for tip of the center baffles with the lower boundary, where was super-critical. The flow is symmetrical, with low velocities at the between the tips of the central baffle, where also the two jets meet and the maximum pool depth is observed. The maximum velocity is observed in the middle of the slot.
For the single slot they modeled different designs, but concluded to similar results, as far as flow conditions are concerned. The first has a slot width of 30 cm. With same

boundary condition upstream and downstream with the double slot design, the flow found to be sub critical, apart from the tip of the long baffle. Between the long baffles an eddy was observed and a stagnation of the flow. The lower water depths were found near the slot and in general lower depths were found near the side wall between the short baffles. In contrast to that at the side wall between the long baffles the higher water depths were found. The maximum velocity was at the center of the slot. The second design 60S, which had a 60 cm slot width, but the same ratio of slot width to pool width. It was found that the results were similar to the 30 design, with the same also critical – sub critical observations. Finally the last design also with a slot width of 60, but with different width ratio of slot to pool, with a bigger discharge had similar response for both boundary conditions. The only difference was that the maximum velocity was observed to be in front of the slot and not at the middle of it. The flow patterns and conditions were similar.

The general conclusions were that the computed maximum velocity is close to the theoretical $Vmax = \sqrt{(2gdh)}$ shown at the center of the slot and getting smaller as it reaches the baffle because of friction. Moreover the velocity distribution is independent of discharge and that most of the pool is in stagnation in the single slots in comparison to the double slot.

Khan (2006) also tried to apply a numerical model on a vertical slot fish way. For Khan vertical velocities must not be ignored, therefore he uses a non-hydrostatic model. Although he made a qualitative model, he wanted to prove that CFD is actually a useful tool in understanding the hydraulics of vertical pool fish-passes and analyze the impacts of the flow on the fish. To accomplish that he used a CFD Code named STAR-CD, solving the Reynolds averaged Navier stokes Equations with a κ-ε turbulence model and pressure downstream boundary conditions. Based on the experimental study of Wu et al. (1999) he created a fish-pass of seven pools based on design 16 of Rajaratnam et al. (1986). The first and last pools and the ones after the first and before the last are characterized by the dependence of the flow from the boundary conditions. The 3 remaining pools showed the same flow conditions; therefore the study was based on the 4th and middle pool. As a result of this study, the flow patterns are similar to the experimental ones from Wu et al. (1999) and Puertas et al. (2007). As far as water depth is concerned, the observations made showed that the lower depth is after the slot, the water rises near the side wall of the long baffles, in contrast to the opposite wall. The highest velocity was observed near the slot, where the jet is forming. After the slot the jet grows and the energy

dissipates. The width of the jet has a relation to the depth. The deeper the narrower is the jet. Near the surface the jet is wider. An eddy is created on both sides of the jet. Khan did not examine the energy of the pool, but the energy need by the fish to pass based on drug coefficient and the size and burst speed of the fish. He concluded, based on other studies that for certain species is suitable and for some it is not.

Alvarez-Vázkez et al. (2007) moved the numerical modeling forward by using also optimization codes to find the best way to design and manage the fish way. They solved the2-D Saint-Venant (shallow water) equations, and then they used the Nelder-Mead algorithm for optimization. For finding the best shape of the vertical slot fish-pass, based on design 6 of Rajaratnam et al. (1986). The used a 10 pool channel with a 5% slope. I order to achieve their goal they had as objective variables, the existence of resting areas within the pool and the maximum water velocity, in order for fish to be able to pass through. The water depth and the averaged mean velocity was obtained by the swallow water equations. The optimization algorithm was searching for the best position in the pool of the long and short baffles, in relation to the pool and between them. They concluded that they optimization algorithm is giving good results in an efficient way, as long as the swallow water equations can be applied.
In their second optimization attempt, they used the same design as above to optimize the incoming water flux, in order for the fish-pass to be attractive to fish. Here the main parameters were the water depth and water velocity of the fish. They found that if the problem is well stated, then the algorithms can be really efficient. They also confirmed their results by making numerical experiments for realistic cases.

One of the most difficult things to numerical calculations is the turbulence model that is going to be used. This is the case, because all of the numerical models are based on empirical and experimental equations, in order to close the Reynolds averaged Navier Stokes equations. Therefore to be really accurate a huge costly mesh is required. For this reason Cea et al. (2007) made an investigation in turbulence models to find which one is more suitable for analyzing the vertical slot fishway flow. He verified his results by using the experimental data from Puertas et al. (2004). He also used the shallow water equations, because from the experiments was shown that the flow is mainly 2-D. The turbulent models that he used were the mixing length model, the κ-ε and the algebraic stress model. They solved the equations for 3 different discharges 35l/s, 65l/s and 105l/s, using an unstructured fine mesh, in a 3

active pool and inlet and outlet pool channel. They got to the conclusion that the flow patterns are close to the experimental ones, but the eddies created by turbulence differ between the turbulence models. Also they checked the results for different bed roughness and they found that it does not play significant role in the flow. As far as the turbulence models are concerned, the ASM and the κ-ε model give good results for the velocity field, and both are sensitive free to the variations of discharge. This was also observed from the experiments. The ML model is sensitive to the variation of discharge. Water depths are generally better predicted from the κ-ε model and the turbulence field from the ASM, while the ML does not give good results. In general the ASM and the κ-ε give similar results, except for the Reynolds stress, which are better predicted from the ASM. With bed slopes greater than 10% the swallow water equations may be not valid to use, therefore the entire above are restricted to this bed slope.

Heimerl et al. (2008) based on the diploma thesis made by Hagmeyer (2005) and Echteler (2006), made also numerical simulations on vertical slot fish-passes. They used two different CFD codes with different characteristics. The one was FENFLOSS, a Reynolds averages Navier Stokes solver and a commercial code ANSYS CFX. The first one simulated, a totally closed filled with water system of a curved fish-pass of design 6 of Rajaratnam et al. (1986) with different arrangements of the short baffles, first from the inner side of the first baffle and then from the outer side. With CFX they created a multi-phase system of 5 pools of design 16 of Rajaratnam et al. (1986). Here different shapes and positioning of guide elements were studied, which proved to be really important to the smoothness of the flow. They concluded that in the change of the position there no significant change, but the main flow is from the opposite side. Moreover they were also in agreement with the experimental data of a 2-dimensional flow and defined that the maximum velocity is observed, not at the center of the slot, but right before it. Furthermore they did not find a uniform velocity distribution to slot from bottom to the surface. The velocity near the bottom is greater than close to the surface. Finally the guide element investigation proved that they play significant role to the flow and their position must be selected with caution, in order to reach the lowest velocity possible.

Motivated by the European directive for fish-passes Chorda et al. (2010) created a numerical model to simulate the flow in vertical slot fish-passes. Because lots of the previous experiments resulted to a 2-D flow in the pool, except the slot region, they decided to solve the Saint Venant equations with the use of κ-εturbulence model.

They also tried to validate the model based on experiments from Poitiers University, France, made with Acoustic Doppler Velocimetry and Particle Image Velocimetry. For the numerical model they used a CFD code, Telemac 2-D with an unstructured triangular mesh. The experimental channel was scaled down, so in order to find possible differences between the scaled mode and the normal one, they run both case in Telemac, but without finding differences since the flow relates to the analogies of the pool. They observed that although a constant value of eddy viscosity does not corresponds well to the flow, the κ-ε model gives good agreement, even if it is overestimating the turbulence field. The flow field was find to be similar to the experimental one, creating a jet flow from the slot and two recirculation areas above and below the jet. Finally some comparisons to the calculated energy dissipation were made. But the flow, the geometry of the baffles and the discharge were too different to be compared with the global dissipated power of Liu et al. (2006).

After observation that the fish have trouble dealing with turning pool in vertical fish-passes, Marriner et al. (2013) created a CFD model to study the flow conditions inside the turning pools. Turning pools are created to connect parallel channels of fish-passes, when the fish-pass connects to sides of high altitude difference. The study was based on field measurements in Vianney Legendre vertical slot fish-pass in Canada. The CFD code, which solved the Reynolds averaged Navier Stokes equations together with the κ-ε turbulence model, gave a flow pattern of a big recirculation in the middle of the pool, with velocities that did not exceed the bursting speed of the fish in use. Those results together with the results of the turbulent flow were in good agreement with the experimental ones and they gave the opportunity to the researchers to observe that there are no resting areas for the fish. Since they found this problem they decided to study more designs of the turning pool through CFD. So they tested 3 new models of the turning pool, with an addition of a baffle wall in different positions in the pool in order to ease the power of the recirculation. Other two models were created changing the bed slope of the pool and finally the last model had a straight back wall, in contrast to all the above. They concluded that the maximum velocities, are not getting higher than the velocity of the fish, which they use the fish-pass. The main problem is the resting space in the turning pool, because it was meant to act as one and this study proved that the hydraulics of the pool are confusing and challenging for the fish. In any case they proposed that the straight back wall pool with the addition of a baffle in the middle, may provide a turning pool with much better hydraulic features.

Following the example of Cea et al. (2007) and having also a CFD code created by them, Bombac et al. (2013) decided to study also the hydraulic features of vertical slot fish-passes with the use of different turbulence models, solving the swallow water equations. They first created a model of a 7 pool vertical slot fish-pass, where they conducted measurements with the use of an Acoustic Doppler Velocimeter and then they simulated with the use of their code. This was a model based on an existing fish-pass in Slovenia. For turbulence they used a constant eddy viscosity model, a Smagorinsky turbulence model and finally κ-ε, which was proved to give good results in previous studies. Their first observation was to confirm that bed roughness is not playing an important role to the flow characteristics. The flow characteristics were also a plane jet form the slot to the long baffle side wall, which goes to the next slot. Between the jet and the two long baffles, a recirculation was created. The maximum velocity was observed at the slot. Furthermore they made some geometrical changes at the pool in order to see how the results will change. They concluded that the CFD is a useful tool to observe the behavior of the flow with small geometrical changes, which can be crucial to the fish preferences. Moreover κ-ε turbulence model turned out to be the best from the tested, since the other two had problems in calculating their necessary coefficients. Really close attention must be paid to the numerical diffusion.

Puzdrowska (2013) made a simulation using the CFD code FLOW 3D, in order to investigate whether the flow conditions in a fish-pass in Poland are appropriate for catadromus fish. Catadromus fish, in contrast to anadromus, can cope with lower maximum velocity and turbulent kinetic energy; they tend to gather near the long baffle and fail to pass to the next pool. The fish-pass that examined consists of two parts. The fist is a vertical slot and the other a bolt fish-pass. She solved the Reynolds averaged Navier Stokes equations and for turbulence she used the κ-ε model. The flow conditions that she calculated, were good for anadromus fish (Salmonoids mainly), but exceeded way too much the limits of catadromus in the biggest part of the pool. In this case the bolt fish-pass showed better efficiency. She concluded that since turbulent kinetic energy is high in the slot section, is a barrier for fish migration and more tests must be conducted in order to define the relation between efficiency for all fish species and turbulent kinetic energy.

Since researchers usually prefer 2-Dimensional solver, Arrowsmith et al. (2014) made a comparison of a 2 dimensional and a 3 dimensional model. The design of the

models was one from the proposed from Zhu et al. (2011) for a technical work in Australia, which has 4 pools and a turning one.
The 2D model was simulated with MIKE 21 from DHI and the 3D with ANSYS CFX. Their aim was to compare water depth, the velocity fields and the energy dissipation factor (P/V). The boundary conditions upstream and downstream were water height. They resulted that the 3d model gives lower by one third the flow discharge and lower velocities and higher water depths upstream as the 2D model. That was the case because of some non-uniformity and non-hydrostatic velocity distribution, which the 2D model does not take under consideration. As far as dissipation is concerned, the dissipation factors calculated from both models were in agreement with the factor lower than the regulation limits. The 3D model though gave a distribution of the energy dissipation factor, from which they observed some areas where the limits exceeded the acceptable values.

Bousmar et al. (2015) created models of two existing fish-passes, one in China and one in Belgium, and tried to verify their CFD models with the experimental values they got. They used the Telemac 2D and Telemac 3D for the fishway in Belgium and ANSYS Fluent 3D and Telemac 3D for the Fishway in China. Their aim was two reproduce programmatically the recirculation patterns and the turbulence levels and parameters. Therefore they used for Telemac the κ-ε model and for Fluent 3D the RNG κ-ε. In the Belgian fish-pass had some agreement with the experimental data in the 2D model and lower accuracy at the 3D model, which was a problem of wrong simulation. In the China fish-pass also had agreement to the measurements with both the 3D and 2D models, without giving more details.

The European laws became very strict with environmental issues, such as fish-passes. Therefore, in the need of creating a new fish-pass in Luebeck Germany, Klein et al. (2015) made a comparison of two types of fishways via numerical simulation. They investigated a weir and a vertical slot fish-pass with the use of Flow 3D program. They used the Large eddy simulation, used for unsteady flow, to calculate directly large eddies and some models for smaller ones. They simulated the whole fish-pass for two discharges. The identified the weir fish-pass as more suitable for the area of investigation, since the velocities were lower and the fish-pass with the given discharges, could maintain the water depth to an acceptable level. Also an eddy generation at the side, with low velocities could work as a resting area for the fish. On the other hand the vertical slot fish-pass gave larger velocities, which next to the guiding baffles were becoming even large, much larger than the acceptable for

the fish of the area. Also with the two discharges chosen, the needed water depth could not be reached. Also in the design of the channel studied, the added a turn, made in several pools. Although the weir fish-pass did not have differences between the pools out of the turn and the pools in the turn, the vertical slot design had significant differences, not only in water depths, but also in velocities. They concluded that although in this case the obvious selection is the weir fish-pass, further study is to be made, in terms of bed roughness and geometrical changes in the channels.

From all the above mentioned researches useful observations on the use of CFD can be made. Generally the vertical slot fish-pass designs are suitable for most of the cases that need such an installation. They are flexible in terms of water discharges and water depths, but in any case are not perfect for every case. The designs that are commonly used are three, the 6, 16 and 18 of Rajaratnam et al.(1992). The use of CFD in solving the flow fields of such a fish way shows good agreement with the experimental data. The only significant problem is the turbulence field, which is difficult to estimate, because of the excessive resources it needs. Therefore lots of observations tend to suggest that the κ-ε turbulent model is in better agreement than the rest. Also the bed roughness found to be a criterion that does not play a significant part in the flow or the water depth, but it needs further investigation. Concluding CFD up to now gives useful guidelines to the researchers and must be a tool in further research, although it has its deficiencies.

Chapter 3. Design of Vertical slot fish-passes

To design a fish-pass is complex and time consuming. Therefore there are two ways that can be used. The first one is the empirical design, based on observations and experiments that have been made on fish-passes and the second is by solving the flow equations, in order to find the flow field. Most of the times an analytical solution is not possible, and it is given through an algebraic repetitive method with the use of a computer system. Although in this study we tried to solve the flow field by solving the Reynolds Averaged Navier Stokes equations, we present also an empirical methodology.

3.1 Empirical Design of Vertical slot fish-passes

In this section an example of empirical design will be given. The methodology consists of 10 steps, based on current literature (Stamou et al.(2015)).

First step is the detection of fish, which are of interest and record their characteristics. In order for this to happen, close collaboration with special-biologist is needed. As far as the main characteristics are concerned, they include the average dimensions and movement speeds that will determine their ability to move against the stream, like in a Fish-pass. Typical values for all kinds of fish can be found in literature.

The second step is to determine the position of the entrance and the exit from the fish-pass. This will determine the water depths at the entrance and at the exit and the discharge of the canal, which are appropriate for the fish of the area of investigation. One of the most important design factors is the water elevation drop ΔH from upstream to downstream.

The next step is to determine the geometrical and hydraulic characteristics in the channel, based again on the fish characteristics. The main factors are the slot width, the mean velocity at the slot and the turbulence factor P. Because the mean slot velocity is the highest velocity in the pool, it is chosen to much the burst speed of the fish. Finally the designer must be cautious to maintain the flow conditions sub-critical, in order to control the flow from downstream conditions. According to experience the maximum velocity at the slot must be between 0.08 and 2.0 m/s. By selecting this velocity we determine the bed slope S and the elevation drop ΔH in every pool from the following mathematical forms.

$$DH = V2/2g \quad \text{(Eq.1)}$$

$$S = DH/Lpool \quad \text{(Eq.2)}$$

Moreover the turbulence factor P, which estimates the turbulent dissipation inside the pool, can be calculated using the following equation.

$$P \approx \frac{\rho \cdot g \cdot \Delta h \cdot Q}{b \cdot h_m \left(l_b - d\right)} \quad \text{(Eq.3)}$$

where is h_m the average depth in the tank,

water density ρ and

g the gravitational acceleration.

The turbulent dissipation factor must be less than a maximum value (Pmax), which makes it difficult for the fish to move and straining, and ranges from 80 up to 200 W/m^3.

The forth step is to calculate the number of pools needed in the channel. This is calculated by the following equation

$$N_{min} = \frac{DH_{max}}{\Delta H} \quad \text{(Eq.4)}$$

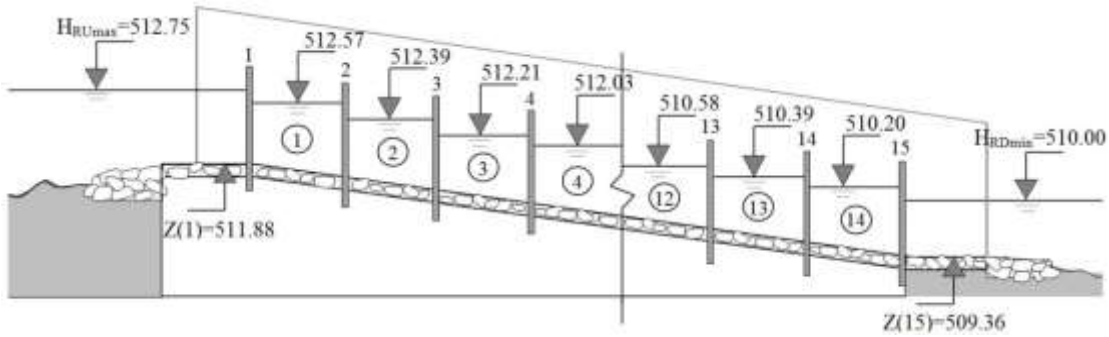

Figure 9 Example of Longitudinal cut of a fish-pass

(Source: Stamou et al. (2015))

Following the number of the pools, the downstream boundary condition must be selected and the water elevation in the pools.The flow is considered to be subcritical throughout the length of Fish-pass, something that will confirm later on, and determine the flow conditions in the last downstream divider wall from which we start hydraulic calculations. In this position we choose for the DI_{max} downstream flow depth equal to $h_{D\,(n+1)} \geq h_{min}$ and determine the water elevation from the bottom, $g_{(n+1)}$, from equation (5)

$Z_{(i-1)}=H_{rdmin} - h_{b(n+1)}$ (Eq.5)

Following that a value $\Delta Z<\Delta H$ for calculating the bed elevation from the reference level is selected and the bed elevation in every baffle is calculated by

$Z_{(i-1)}=Z_{(i)}+\Delta Z$ (Eq.6)

Next step is the hydraulics calculations. The calculations are based upon 4 equations.

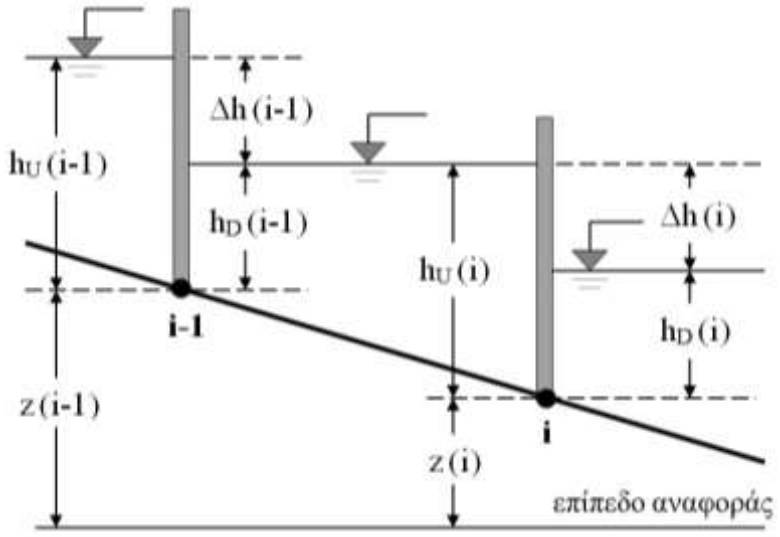

Figure 10 Geometrical Characteristics of the Fish-pass

(source: Stamou et al. (2015))

These 4 equations calculate the energy upstream and downstream of a baffle, the energy between the upstream and downstream of a pool, the slot discharge and the μ coefficient, which calculates a discharge, for which the energy at the first baffle is equal to H_{rumax}.

3.2 Computational Fluid Dynamics Software

Computational fluid dynamics software (CFD) solves the flow field equations together with a turbulence model. The continuity and momentum equations are solved to determine the 3-D flow field in the Fish-Pass and the free surface is determined with the Volume of Fluid (VOF). In this study, with the use of FLOW-3D we solved the Reynolds Averaged Navier Stokes (RANS) equations with a use of Renormalization Group k-epsilon turbulence model as a closure model. Finally the algebraic method that is used to discretize the differential flow field equations is the Finite Volume Method.

3.2.1 Flow field equations

The continuity and momentum equations in a Cartesian coordinate system read as follows:

$$V_F \frac{\partial \bar{\rho}}{\partial t} + \frac{\partial}{\partial x^i}\left(\bar{\rho}\overline{u^i}A^i\right) + \frac{\partial}{\partial x^j}\left(\bar{\rho}\overline{u^j}A^j\right) = 0 \qquad \text{(Eq.7)}$$

$$\frac{\partial \overline{u^i}}{\partial t} + \frac{1}{V_F}\left(\overline{u^i}A^i\frac{\partial \overline{u^i}}{\partial x^i} + \overline{u^j}A^j\frac{\partial \overline{u^i}}{\partial x^j}\right) = -\frac{1}{\bar{\rho}}\frac{\partial P}{\partial x^i} + G^i + f^i \qquad \text{(Eq.8)}$$

where V_F is the fractional volume open to flow, $\bar{\rho}$ is the bulk density of water-SS mixture, t is the time, P is the pressure, x^i is the Cartesian coordinate in the i-direction, $\overline{u^i}$ is the bulk velocity of water-SS mixture,A^i is the fractional area open to flow, $G^i$is the body acceleration and f^i is the viscous acceleration in i-direction.

The viscous accelerations are calculated by:

$$\bar{\rho}V_F f^i = \tau_{bx^i} - \left[\frac{\partial}{\partial x^i}\left(A^i\tau_{x^ix^i}\right) + \frac{\partial}{\partial x^j}\left(A^j\tau_{x^ix^i}\right)\right] \qquad \text{(Eq.9)}$$

Where$\tau_{bx}{}^i$ is the wall shear stress and $\tau_{x}{}^{i}{}_{x}{}^{i}$ is the strain rate tensor; the latter are calculated

$$\tau_{x^ix^i} = -2\mu_{tot}\left(\frac{\partial \overline{u^i}}{\partial x^i}\right) \qquad \text{(Eq.10)}$$

$$\tau_{x^ix^j} = -\mu_{tot}\left(\frac{\partial \overline{u^i}}{\partial x^j} + \frac{\partial \overline{u^j}}{\partial x^i}\right) \qquad \text{(Eq.11)}$$

Where $\mu_{tot}=\mu+\mu_T$ is the total dynamic viscosity, μ is the dynamic viscosity and μ_T is the eddy viscosity.

The eddy viscosity is calculated via the turbulence renormalization-group (RNG) model, which is based on the eddy viscosity hypothesis and applies statistical methods for the derivation of the averaged equations for the turbulence kinetic energy (k) and the turbulence dissipation (ε). Moreover, it uses similar equations to the standard k-ε model. However, additional terms exist and model constants differ, as they are derived explicitly and not empirically, as in the standard k-ε model. In

general, the RNG model has wider applicability and it is known to describe low intensity turbulence flows and flows having strong shear regions more accurately than the standard k-ε model. The distributions of k and ε are calculated by Eq. 12 and Eq. 13:

$$\frac{\partial(\bar{\rho}k)}{\partial t}+\frac{1}{V_F}\left(\bar{\rho u^i}A^i\frac{\partial k}{\partial x^i}+\bar{\rho u^j}A^j\frac{\partial k}{\partial x^j}\right)=P_s+G+Diff-\bar{\rho}\varepsilon \qquad \text{(Eq.12)}$$

$$\frac{\partial(\bar{\rho}\varepsilon)}{\partial t}+\frac{1}{V_F}\left(\bar{\rho u^i}A^i\frac{\partial \varepsilon}{\partial x^i}+\bar{\rho u^j}A^j\frac{\partial \varepsilon}{\partial x^j}\right)=\frac{1.42\varepsilon}{k}(P_s+0.2G)+DDif\text{-}1.68\frac{\bar{\rho}\varepsilon^2}{k} \qquad \text{(Eq.13)}$$

where P_s represents the shear production, G is the buoyancy production and Diff and DDif represent the diffusion.

3.2.2 The Volume of Fluid model

The free surface is handled by the VOF method [19] that determines the volume fraction (F). In this method the cells of fluid domain are classified as empty, fully filled or partially filled with fluid and the corresponding volume fraction (F) varies from 0 (empty cells) to 1 (fully filled cells); F is determined by the following transport equation:

$$\frac{\partial F}{\partial t}+\frac{1}{V_F}\left[\frac{\partial}{\partial x^i}\left(FA^i\bar{u^i}\right)+\frac{\partial}{\partial x^j}\left(FA^j\bar{u^j}\right)\right]=0 \qquad \text{(Eq.14)}$$

The VOF method consists of three components: a scheme to locate the surfaces, a method to track surfaces and a process to set the appropriate boundary conditions. In each cell of the computational grid, the value of F is calculated, then it is compared with the values of F in the surrounding cell volumes, and finally the surface slope and the position of water surface are determined.

Chapter 4. Numerical and Calculation Details

The purpose of this work is to verify a 3D computational fluid dynamics model for a vertical slot fish-pass with the use of experimental data presented by Puertas et al.(2004).

Puertas et al.(2004) made an attempt to continue the research that started from Rajaratnam et al.(1992) and Wu et al.(1999). The first team concluded in 1992 that there are 3 appropriate designs for vertical slot fish-passes that are suitable for most fish cases and can be used by most of the fish types. Wu et al.(1999) made a detailed study on one of the proposed design with 3 different bed slopes and several discharges. Puertas et al.(2004) made experimental measurements on the other two designs, for 2 different bed slopes. According to Wu et al.(1999),for bed slope 5% the main flow is a two-dimensional curved jet and for 10% and above is three dimensional. For this reason Puertas et al.(2004) chose the bed slope to be near these values. The first was 5.7% and the second 10.05%.

4.1 Geometry of the pass

The experiment took place at the Centro de Innovacion Tecnoloxica en Edificacion e Inxeneria at the University of Coruna, Spain. A scaled model of a fish-pass was created, consisted of a metallic structure 12m long, which was able to change the bottom slope. It was divided to 11 pools. The first and the last pool were for inflow and outflow respectively and were smaller. The first four pools, after the head tank, were of design T2, then followed an intermediate pool and then 4 pools of design T1. All the walls were made of Plexiglas, in order to observe the flow. Measurements were made in pools 3 and 7, as shown to the figure below. The discharge was measured with an electromagnetic flow meter. The baffles were always vertical despite the slope of the bed. The dimension of the pools were as proposed by Larinier et al.(1998) with slight differences, in order to adapt to the infrastructure of the existing facilities.

A Cartesian positioner was placed over the experimental pools, in order to automate the positioning of the measurement instruments. Therefore the instruments can be set automatically at any point in the pool creating a three dimensional mesh.

Two measurement devices were placed on the Cartesian positioner, which were a depth probe and ADV velocimeter.Velocities were measured by means of a Doppler Effect velocimeter (MicroADV). The MicroADV is a drift free device, which means that

no calibration is needed, in contrast to the depth probe that needed calibration every working day.

Velocity measurements were made in planes parallel to the bed with 10 cm distance between them, starting at 5 cm to as close as possible to the water surface. The data points eventually created a data mesh of 10x10, which was becoming finer at critical areas.

The water surface was measured with a conductivity-based depth probe. The depth measurements were evaluated by a bi-dimensional mesh of 10x10x10.

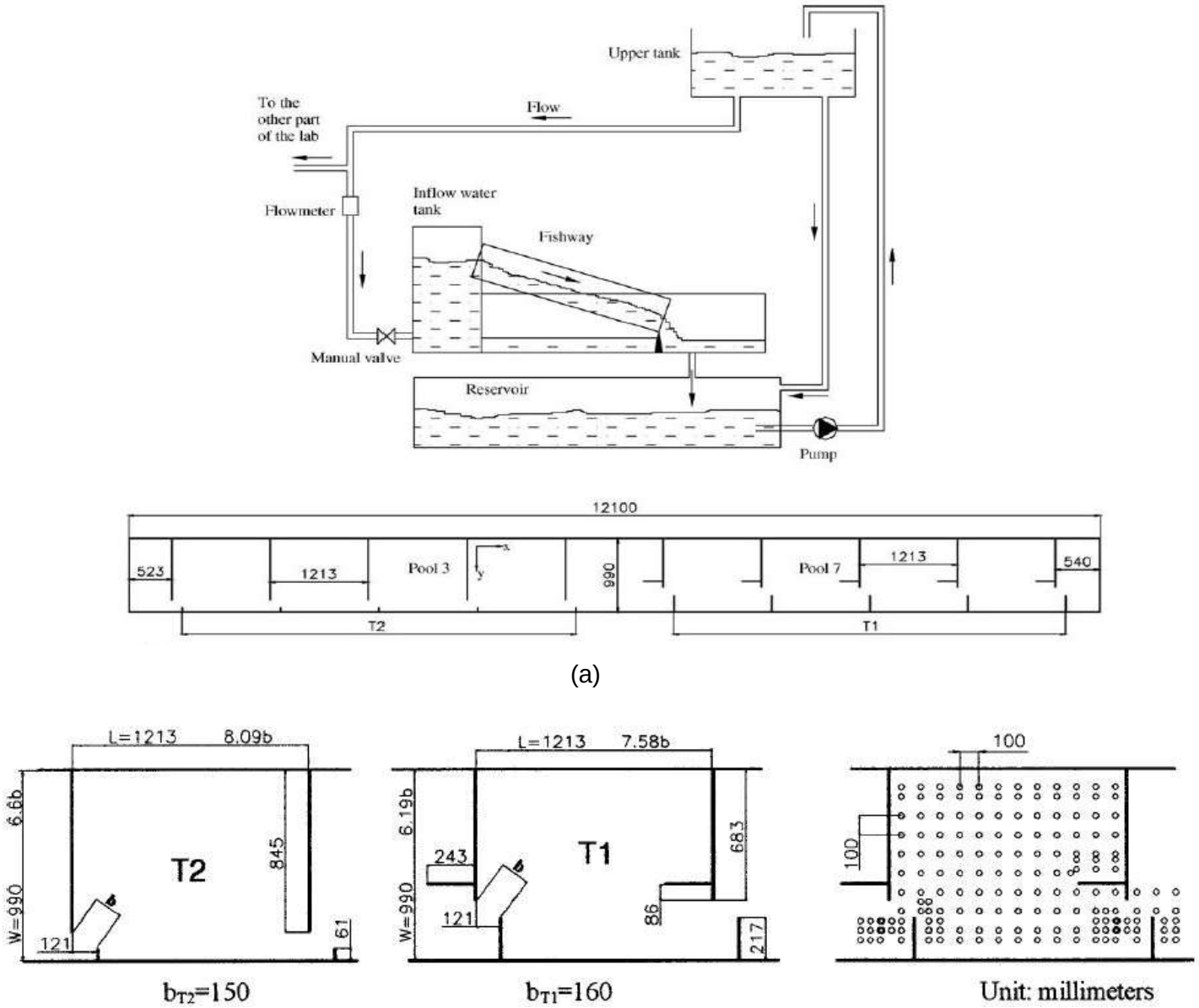

Figure 11 Experimental Fish-Pass (a) Top view and (b) pool design T1 and T2

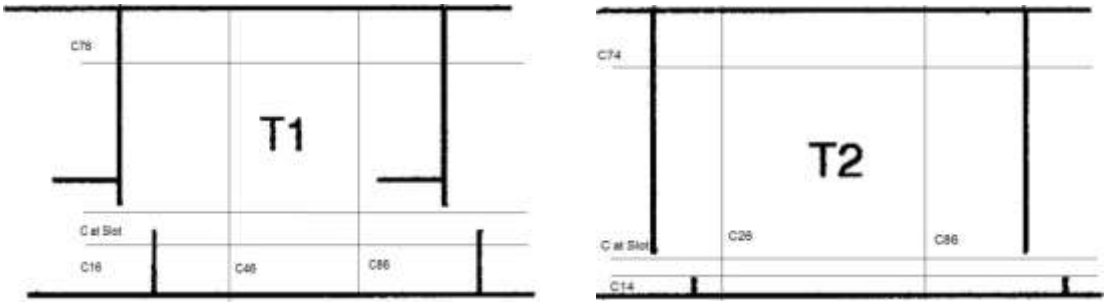

Figure 12 Cross Sections for Pool designs T1 and T2

The measurements that were obtained from the experiments are presented to the table below.

Table 1. Experimental Measurements by Puertas et al.(2004)

Design	So	Q (m3/s)	QA	Yo (m)	Yb (m)	Ym (m)	Ymax (m)	Ymin (m)	Vb (m/s)	Cd	Ed(W/m3)
TI	5.7	0.0159	0.4945	0.125	0.158	0.130	0.175	0.107	0.860	0.730	71.81
TI	5.7	0.0209	0.6529	0.176	0.195	0.179	0.215	0.143	0.850	0.790	67.13
TI	5.7	0.0246	0.7669	0.190	0.230	0.197	0.236	0.167	0.790	0.850	72.99
TI	5.7	0.0341	1.0624	0.253	0.306	0.262	0.313	0.212	0.880	0.800	75.94
TI	5.7	0.0458	1.4277	0.379	0.406	0.386	0.425	0.356	0.840	0.830	68.25
TI	5.7	0.0540	1.6827	0.437	0.476	0.445	0.483	0.400	0.870	0.820	69.74
TI	5.7	0.0641	1.9983	0.488	0.529	0.495	0.540	0.453	0.890	0.850	74.18
T1	5.7	0.0741	2.3104	0.604	0.604	0.608	0.652	0.562	0.880	0.870	69.35
T1	5.7	0.0859	2.6791	0.665	0.697	0.674	0.711	0.628	0.850	0.910	72.97
T1	10.05	0.0348	1.0847	0.155	0.201	0.171	0.253	0.093	1.250	0.860	223.25
T1	10.05	0.0445	1.3879	0.247	0.278	0.262	0.357	0.178	1.200	0.830	179.76
T1	10.05	0.0551	1.7174	0.314	0.371	0.331	0.420	0.242	1.210	0.770	174.88
T1	10.05	0.0643	2.0059	0.366	0.406	0.378	0.469	0.288	1.190	0.830	175.00
T1	10.05	0.0751	2.3425	0.436	0.505	0.452	0.541	0.363	1.250	0.750	171.72
T1	10.05	0.0849	2.6482	0.489	0.553	0.507	0.597	0.429	1.000	0.960	172.94
T1	10.05	0.0945	2.9478	0.526	0.561	0.541	0.634	0.443	1.170	0.900	179.16
T1	10.05	0.1044	3.2554	0.581	0.621	0.596	0.690	0.513	1.050	1.010	179.11
T1	10.05	0.1150	3.5856	0.641	0.681	0.656	0.755	0.556	1.060	1.000	178.79
T2	5.7	0.0160	0.5855	0.102	0.107	0.109	0.152	0.061	0.950	1.050	88.18
T2	5.7	0.0250	0.9153	0.169	0.184	0.180	0.225	0.122	0.930	0.970	83.64
T2	5.7	0.0350	1.2811	0.263	0.278	0.274	0.323	0.214	0.990	0.840	75.23
T2	5.7	0.0453	1.6585	0.350	0.376	0.362	0.408	0.298	1.000	0.810	72.96
T2	5.7	0.0540	1.9772	0.439	0.456	0.449	0.497	0.376	0.970	0.820	69.39

T2	5.7	0.0639	2.3405	0.524	0.539	0.531	0.577	0.475	1.090	0.720	68.82
T2	5.7	0.0741	2.7131	0.606	0.618	0.613	0.660	0.552	0.870	0.920	69.02
T2	5.7	0.0840	3.0785	0.670	0.711	0.679	0.732	0.615	0.960	0.820	70.81
T2	10.05	0.0253	0.9277	0.134	0.197	0.138	0.208	0.080	1.140	0.750	188.43
T2	10.05	0.0352	1.2912	0.206	0.242	0.202	0.276	0.132	1.230	0.790	170.20
T2	10.05	0.0453	1.6601	0.248	0.292	0.251	0.329	0.152	1.320	0.790	181.73
T2	10.05	0.0549	2.0100	0.307	0.346	0.311	0.405	0.212	1.320	0.800	177.95
T2	10.05	0.0645	2.3644	0.371	0.399	0.372	0.461	0.275	1.270	0.850	173.48
T2	10.05	0.0746	2.7325	0.431	0.459	0.432	0.515	0.330	1.310	0.830	172.42
T2	10.05	0.0838	3.0718	0.483	0.509	0.480	0.569	0.380	1.330	0.830	172.81
T2	10.05	0.0954	3.4955	0.536	0.575	0.539	0.623	0.437	1.300	0.850	177.17
T2	10.05	0.1048	3.8398	0.578	0.616	0.578	0.657	0.483	1.300	0.870	180.66
T2	10.05	0.1151	4.2177	0.615	0.657	0.612	0.714	0.505	1.460	0.800	186.50
T2	10.05	0.1248	4.5739	0.650	0.712	0.649	0.745	0.536	1.280	0.910	191.39

4.2 Simulation using swallow water equations

As mentioned earlier Cea et al.(2007),based on the experiments from Puertas et al.(2004), made a numerical simulation of the fish-pass. Their aim was to assess the possibility of using the depth averaged shallow water equations with several turbulence models. They used the Mixing Length model (ML), the k-epsilon, based on the eddy viscosity hypothesis, and the Algebraic Stress Model (ASM). They made the calculation only for one bed slope o0f 10%. They concluded that their results were satisfactory when using both the k-epsilon model and the ASM, with k-epsilon being slightly worse at calculating the Reynolds stresses.

4.3 Simulation using Flow 3-D

In order to investigate the effect of discharge and bottom slope, we designed the whole experimental fish-pass in Flow 3D, following the dimensions given by Puertas et al. (2004), and performed calculations in the same pools of the canal were they conducted the experiment. We created 6 scenarios, three for every pool design; in the first 4 scenarios we used bed slope of 10.05 % and two different discharges of 65 l/s and 105 l/s and in the last two we changed the bed slope to 5.74% and performed calculations for a discharge of approximately 65 l/s.

Table 2. Scenarios of calculation

Scenario	Pool design	Slope (%)	Q (L/s)
T11	T1	5.7	65
T12	T1	10.0	65
T13	T1	10.0	105
T21	T2	5.7	65
T22	T2	10.0	65
T23	T2	10.0	105

4.3.1 Setup of FLOW-3D

The setup of the CFD software consists of the creation of the model, the creation of the mesh, with the boundary conditions and by setting the initial conditions to the program.

The model was created fully in FLOW-3D, although generally is much simpler in a cad software, because it consisted of a solid bottom plate and vertical baffles. Here must be noted that because the experiment was a scaled model, the vertical walls were too thin to be design as solid objects, so they were made as baffles. The bottom roughness was not taken into account and we used the 0 value, because of the Plexiglas material of the bed and walls, and because in the literature, all numerical studies that have been made, concluded that it does not play significant role in the results. We can see the model in figure…

The mesh was orthogonal structured rectangular separated in 6 blocks in order to simulate the t bed slope of the canal. It uses also the Fractional Area-Volume obstacle representation (FAVOR) in order to eliminate stair step effect by blocking out fractional portions of grid cell faces and volumes. Also there was a thickening of the mesh in positions of interest, such as walls and the slot. For boundary conditions we used the volume flow rate, which keeps the discharge in inlet steady and at the outlet we used specific pressure, to imitate a huge water tank that it is not affected by the water from the canal.At the model design, we did not use side walls because we did not have wall roughness and we used boundary condition at the mesh that is

wall. The rest was the default for the program “symmetry”, which is a Neumann condition that wants to show the continuity beyond the mesh and between the blocks.

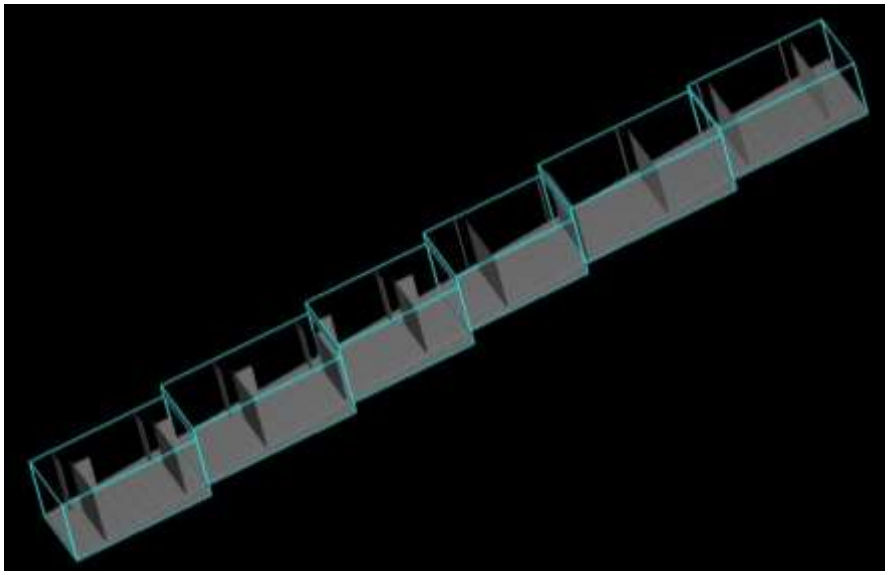

(a) Favor Model with the outline of the rectangular mesh

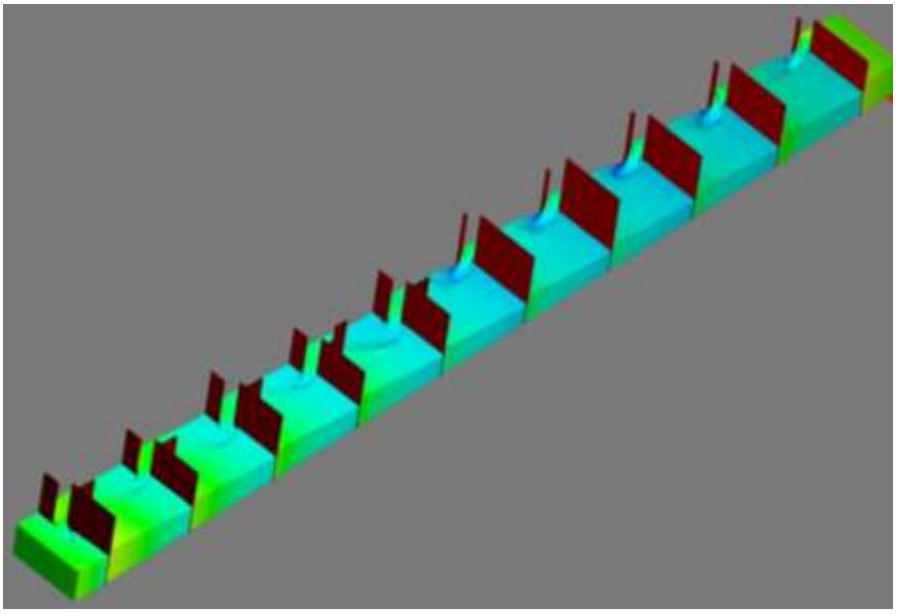

(b) The model filled with water after the end of the simulation

Figure 13 The simulated Fish-pass as a model in FLOW – 3D

4.3.2 Mesh independence study

In general the creation of the mesh is really important in CFD, because the mesh is responsible for good quality results. Generally small meshes converge quickly but

are not able to give correct solutions. That's why we need always an independence study, to prove that the solution that a mesh gives is independent from the size of the mesh.

In this study we created 3 different meshes in flow 3D, the first with one million cells, the second with two million cells and the last with almost three million cells. The results can be seen in the figures below. Generally we concluded that the second mesh was reasonably good, because it gave similar results with the finer one and better than the rough one. The correlation coefficient between the fine and the medium mesh, which we selected, is calculated 0.99. And all that in a low computation cost in comparison with the fine one.

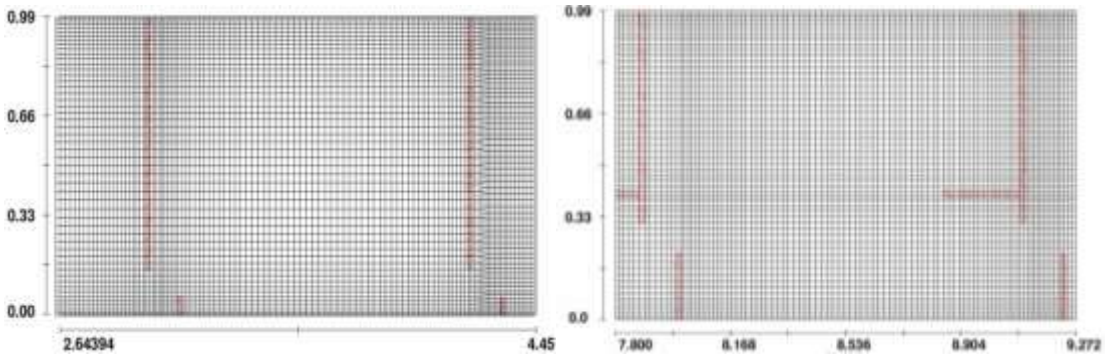

(a) Mesh for Design T2 (b) Mesh for Design T1

Figure 14 Detail of Numerical Meshes

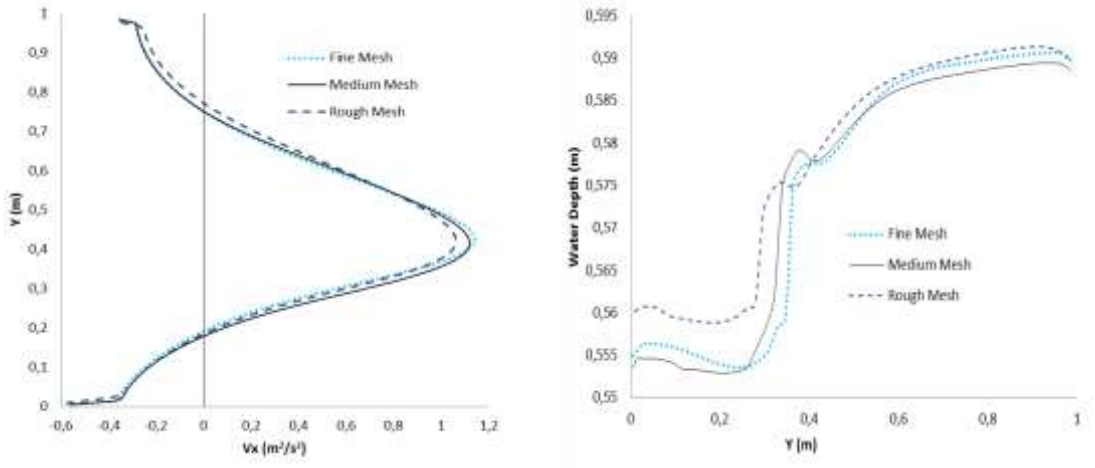

(a) Longitudinal Velocity V_x (m/s) (b) Water Depth (m)

Figure 15 Mesh Convergence. Q=105 l/s, S_o=10%, Design T1

Chapter 5. Results

The results that we obtained from the several simulations can be separated in three major categories; the flow field, which gives as the velocity magnitude and the flow patterns, the water depth and the turbulence field. But before we see the results in each category, we can have a general idea of the results by comparing the experimental measurements from Puertas et al.(2004) at table 1 and the results we obtained from the simulation. As we can see the relative error calculated separately for each value is very low, which means that the simulation calculates satisfactorily water depth and velocity field.

5.1 Statistics

5.1.1 Correlation Coefficient

The correlation coefficient r measures the strength and direction of a linear relationship between two variables. r is always between +1 and –1 The minus sign shows that there is a linear downhill relation, while the plus sign an uphill relation. To interpret the value taken, see table below:

Value	Relationship
± 1	Perfect
± 0.70	Strong
± 0.50	Moderate
± 0.30	Weak
0	No relationship

R is determined by :

$$r = \frac{\sum_{i=1}^{n}(O_i - \bar{O})(P_i - \bar{P})}{\sqrt{\sum_{i=1}^{n}(O_i - \bar{O})^2}\sqrt{\sum_{i=1}^{n}(P_i - \bar{P})^2}}$$

5.1.2 Coefficient of determination

The coefficient of determination, symbolized by R^2 or r^2, is an index that indicates the proportion of the variance in the dependent variable that is predictable from the independent variable.

It is a statistic used in models whose main purpose is the prediction of an outcome or the testing of hypotheses, on the basis of other related information. It shows how well measurements are replicated by a model, based on the proportion of total variation of outcomes explained by the model.

The coefficient of determination ranges from 0 to 1. Values of R^2 outside the range 0 to 1 can occur where it is used to measure the agreement between observed and modeled values and where the "modeled" values are not obtained by linear regression and depending on which formulation of R^2 is used.

5.1.3 RMSE

The root-mean-square error (RMSE) is a measure that uses the differences between values (sample and population values) predicted by a model and the values measured at an experiment. The RMSE represents the sample standard deviation of the differences between calculated values and measured values. These differences are called residuals when the calculations are performed over the data sample that was used for estimation, and are called prediction errors when computed out-of-sample. The RMSE serves to cluster the magnitudes of the errors in calculations for various times into a single index of predictive power. RMSE is a good measure of accuracy, but only to compare predicted measurements errors of different models for a particular variable and not between variables, as it is scale-dependent. The RMSE formula is

$$RMSE = \sqrt{\frac{1}{n}\sum_{i=1}^{n}(O_i - P_i)^2}$$

5.1.4 MAPE

The mean absolute percentage error (MAPE) is an index of prediction accuracy of a forecasting method in statistics. It is an index of accuracy as a percentage, and is expressed by the following formula:

$$MAPE = \frac{100}{n}\sum_{i=1}^{n}\left|\frac{O_i - P_i}{O_i}\right|$$

where O is the observed value and P is the forecast value.

Although the concept of MAPE sounds very simple and convincing, it has major drawbacks in practical application. It cannot be used if there are zero values because there would be a division by zero.
For forecasts which are too low the percentage error cannot exceed 100%, but for forecasts which are too high there is no upper limit to the percentage error.
When MAPE is used to compare the accuracy of prediction methods it is biased in that it will systematically select a method whose forecasts are too low.

5.1.5 Index of Agreement

Index of agreement is a statistic proposed by Willmott and Wicks (1980) and Willmott (1981) that measures how accurate are the predictions of a model compared to accurate and reliable observations. It supposes that The predictions P and the observations O have the same units. The upper limit is 1.0 and indicates perfect model performance. The form of the Index of Agreement (d) is

$$d = 1 - \frac{\sum_{i=1}^{n}|(P_i - O_i)^2|}{\sum_{i=1}^{n}(|P_i - \bar{O}| + |O_i - \bar{O}|)^2}$$

Modified index of agreement (d_1) was introduced by Willmott et al., (1985), when they realized that by squaring the differences, they over-weight the largest error, something that for model with similar performance is not ideal. Therefore the d_1 is based upon the differences of absolute values. The advantage is that d_1 reaches 1.0 slower than d, and is a better index for similar performance models. The form of d_1 is

$$d_1 = 1 - \frac{\sum_{i=1}^{n}|P_i - O_i|}{\sum_{i=1}^{n}(|P_i - \bar{O}| + |O_i - \bar{O}|)}$$

5.2 General Results

The first results to be compared are the experimental results given by Puertas et al.(2004) for the cases that we run. The results are given to table 3, together with the relative error of the measured with the calculated values. The values compared are Y_o, which is the mean depth of the pool, the Y_m which is the mean depth at the central cross section cut, the Y_b, which is the mean depth at the slot, Y_{max} and Ymin , which are the max and min pool depths and V_b, which is the depth averaged mean velocity at the slot region. From Table 3 we can see that the relative error is low and in most cases lower than ± 5%, which indicates that the results calculated are in

good agreement with the measurements. As far as the mean slot velocity is concerned, the values have a significant difference, but it is between the upper and lower limits of the calculated velocity.

Table 3. Comparison of experimental measurements and calculated values

	Scenario 11			Scenario 12			Scenario 13		
	Q=65 l/s, S=5,75% , T1			Q=65 l/s, S=10% , T1			Q=105 l/s, S=10% , T1		
	Experimental	Calculated	Relative Error	Experimental	Calculated	Relative Error	Experimental	Calculated	Relative Error
Ymax	0,54	0,55	-2,43%	0,469	0,47	0,85%	0,69	0,65	5,22%
Ymin	0,45	0,46	-0,44%	0,288	0,29	-1,74%	0,51	0,49	4,87%
Yo	0,49	0,50	-2,66%	0,366	0,37	-2,08%	0,58	0,57	2,58%
Ym	0,50	0,51	-2,02%	0,378	0,38	0,17%	0,60	0,57	4,03%
Yb	0,53	0,50	4,73%	0,406	0,39	4,19%	0,62	0,59	4,77%
Vbmean	0,89	0,93	-4,49%	1,19	1,08	9,24%	1,05	1,13	-8,00%
Vb min		0,73	17,53%		0,85	28,57%		0,87	17,14%
Vb max		1,06	-19,33%		1,19	0,00%		1,27	-20,95%

	Scenario 21			Scenario 22			Scenario 23		
	Q=65 l/s, S=5,75% , T2			Q=65 l/s, S=10% , T2			Q=105l/s, S=10% , T2		
	Experimental	Calculated	Relative Error	Experimental	Calculated	Relative Error	Experimental	Calculated	Relative Error
Ymax	0,58	0,57	1,80%	0,46	0,47	-1,52%	0,66	0,67	-2,51%
Ymin	0,48	0,45	4,63%	0,28	0,27	0,36%	0,48	0,48	-0,29%
Yo	0,52	0,51	3,05%	0,37	0,38	-2,43%	0,58	0,58	0,10%
Ym	0,53	0,51	4,16%	0,37	0,38	-2,42%	0,58	0,58	0,03%
Yb	0,54	0,52	4,27%	0,40	0,39	3,01%	0,62	0,59	4,94%
Vbmean	1,09	1,02	6,42%	1,27	1,16	8,35%	1,30	1,30	0,15%
Vb min		0,51	53,03%		0,49	61,18%		0,58	55,69%
Vb max		1,30	-19,29%		1,44	-13,31%		1,56	-20,00%

5.3 Flow Field

The flow field consists of a main jet, which runs the pool from the inlet slot to the outlet one, and two recirculation areas. One of the recirculation areas is between the long baffles and is the bigger one and the other is between the short baffles and is smaller. Both are characterized by the low velocities in these areas. The higher velocities are at the slot region, where the jet forms, and the maximum velocity is right after the inlet slot.

In general the flow field at pool design T2 was find as proposed by Puertas et al.(2004). For the flow field of T1 though, Puertas et al. (2004) have proposed two flow patterns, which depend on the size of the discharge. Although we managed to confirm the flow pattern for lower discharges, this did not occur to the pattern proposed for higher discharges. This may occur due to numerical error at the solution or the in ability of the turbulence closure model RNG k-ε.

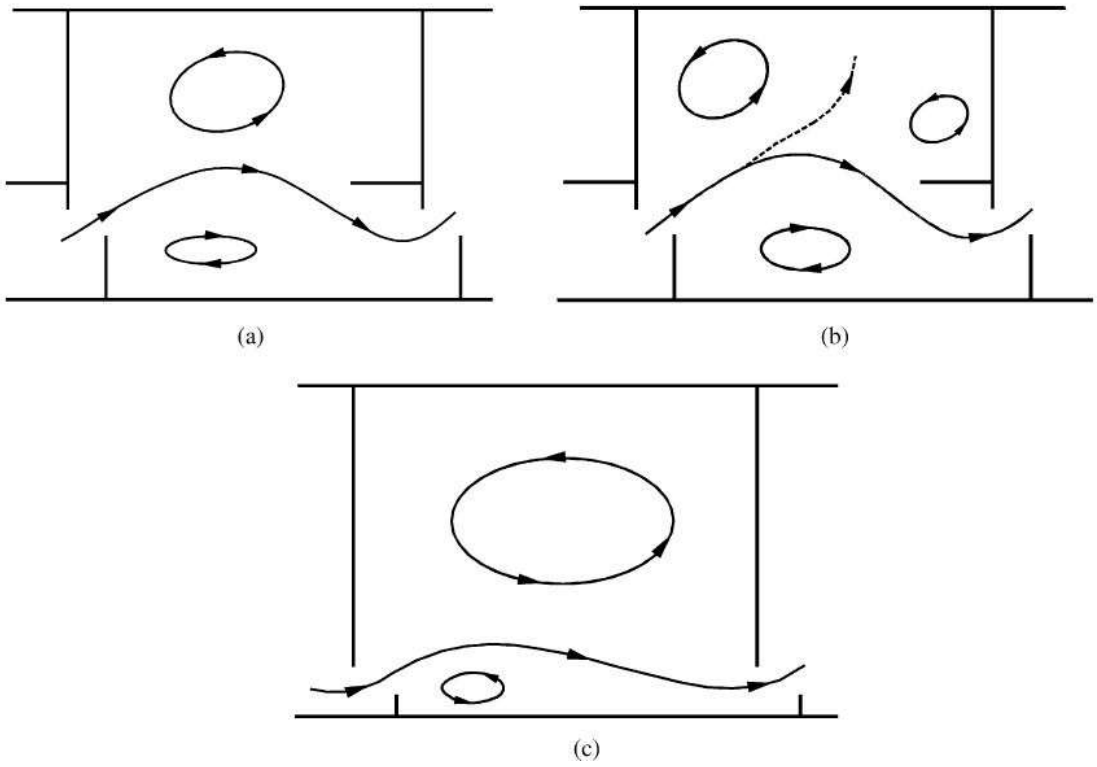

Figure 16 Flow Field Patterns from Puertas et al.(2004)

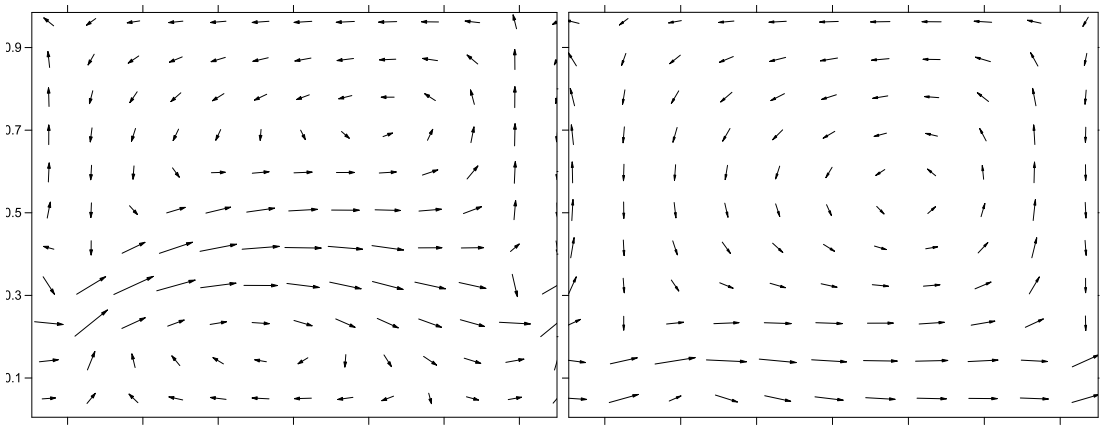

(a) T11 Vx-Vy Magnitude

(b) T21 Vx-Vy Magnitude

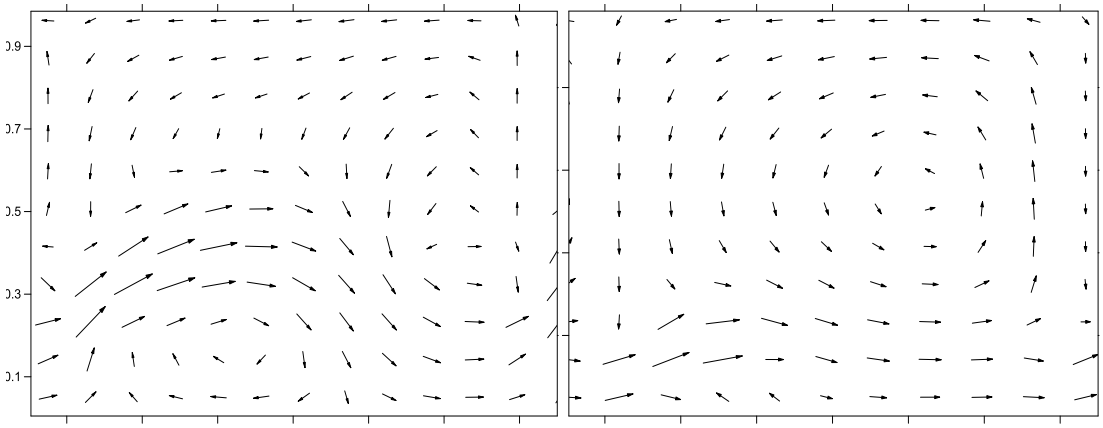

(c) T12 Vx-Vy Magnitude

(d) T22 Vx-Vy Magnitude

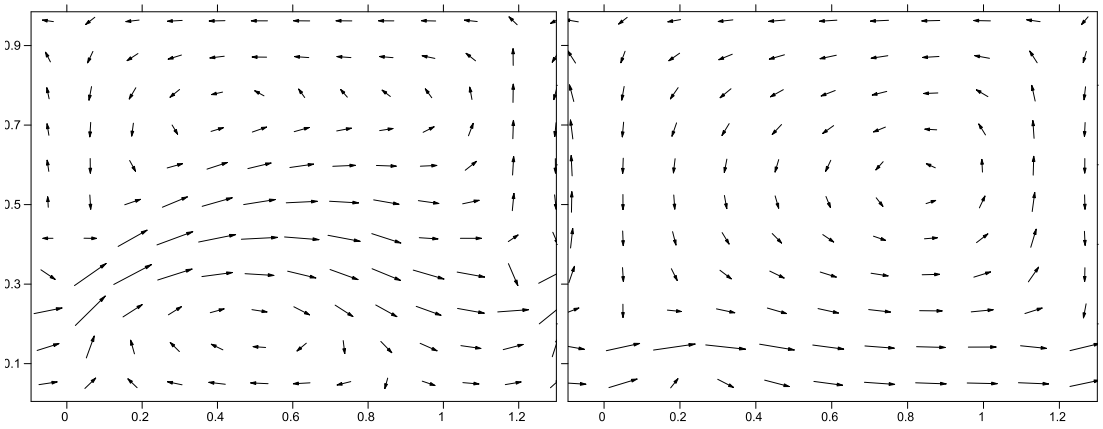

(e) T13 Vx-Vy Magnitude (f) T23 Vx-Vy Magnitude

Figure 17 Horizontal velocity fields Vx-Vy for the scenarios of the present model

Except for the flow field, a comparison were made also to the depth averaged velocity fields obtained from the measurements and computed from the present numerical model and the k-ε numerical model of Cea et al.(2007). As we can observe both numerical models give similar results, with the k-ε, to be more accurate than the RNG for both designs near the downstream wall. Near the upstream wall though the velocity field results are quite similar with the RNG giving slightly better results at the jet area.

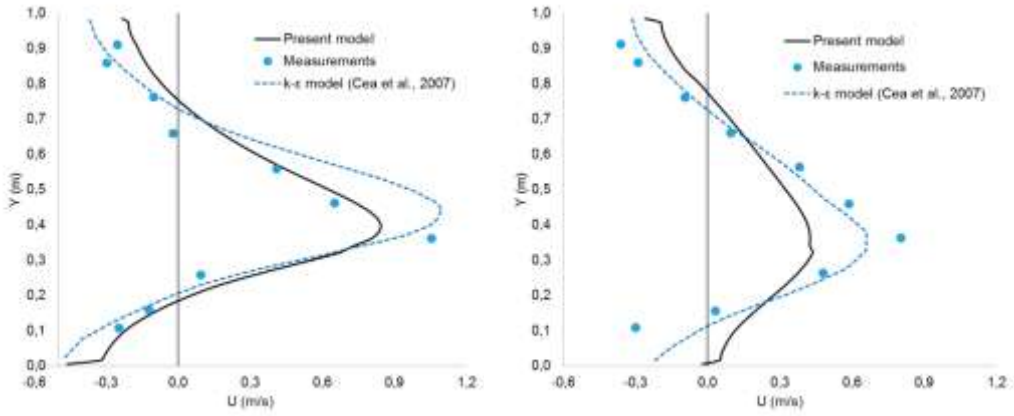

(a) T12 at section C46 (b) T12 at section C86

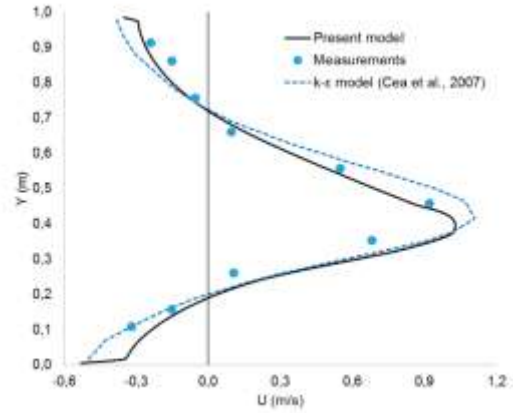

(c) T13 at section C46

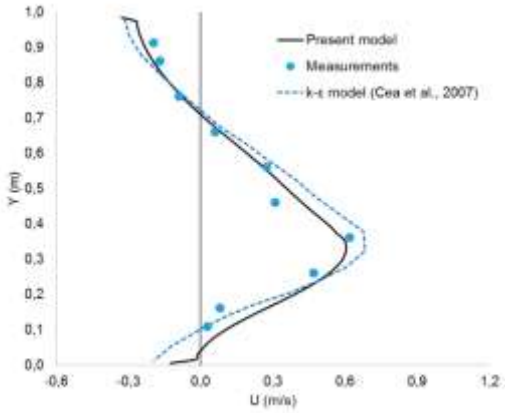

(d) T13 at section C86

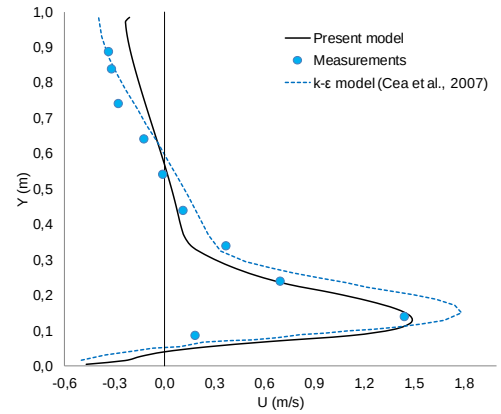

(e) T22 at section C46

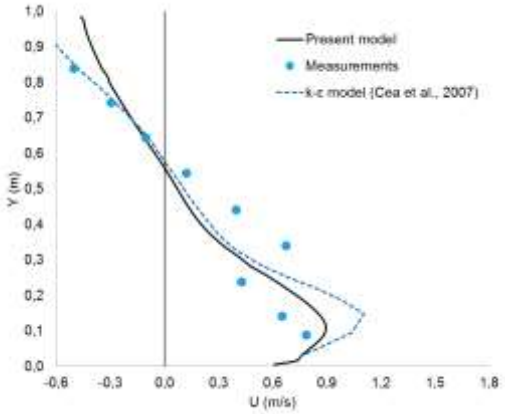

(f) T22 at section C86

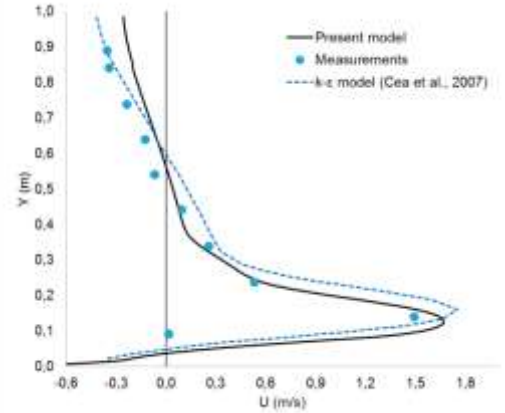

(g) T23 at section C46

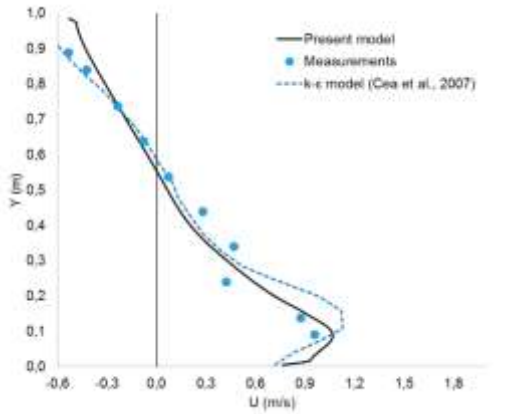

(h) T23 at section C86

Figure 18 Comparison of longitudinal velocities at various cross sections for scenarios T12, T13, T22 and T23

Table 4. Statistic comparison of measurements with the models for the longitudinal velocities for Scenarios of Design T1

	Flow Field - Velocity Vx							
	Scenario T12				Scenario T13			
	C=46		C=86		C=46		C=86	
	Present Model	k-ε Cea et al(2007)	Present Model	k-ε Cea et al(2007)	Present Model	k-ε Cea et al(2007)	Present Model	k-ε Cea et al(2007)
Correration of Determination	0,930	0,874	0,846	0,949	0,926	0,976	0,931	0,965
MAPE	150,74%	169,44%	106,79%	62,13%	50,48%	56,98%	73,23%	44,61%
RMSE	0,144	0,199	0,225	0,120	0,125	0,133	0,083	0,088
Index of Agreement	0,966	0,952	0,846	0,970	0,977	0,979	0,976	0,976
Modified Index of Agreement	0,817	0,803	0,615	0,842	0,865	0,859	0,865	0,854

Table 5. Statistic comparison of measurements with the models for the longitudinal velocities for Scenarios of Design T2

	Flow Field - Velocity Vx							
	Scenario T22				Scenario T23			
	C=46		C=86		C=46		C=86	
	Present Model	k-ε Cea et al(2007)	Present Model	k-ε Cea et al(2007)	Present Model	k-ε Cea et al(2007)	Present Model	k-ε Cea et al(2007)
Correration of Determination	0,732	0,924	0,614	0,610	0,616	0,833	0,959	0,957
MAPE	107,11%	125,97%	38,48%	36,33%	39,88%	57,64%	28,37%	20,71%
RMSE	0,321	0,250	0,193	0,223	0,445	0,325	0,102	0,143
Index of Agreement	0,907	0,954	0,957	0,953	0,847	0,921	0,852	0,878
Modified Index of Agreement	0,782	0,813	0,799	0,814	0,740	0,772	0,754	0,724

From the statistic indexes we can see that both models are strongly correlated to the measurements. In most cases the present model is slightly better, in most of the coefficients. Although we see that there are contradictions between the statistical indexes, this is normal in models where the performance is similar. That is why we present 6 indexes.

In general we can add that more or less the present model gives better results for the scenarios of design T1 and the k-epsilon for the results of design T2.

5.4 Water Depth

As proven by Cea et al., (2007) the numerical models predict the water depth distribution satisfactorily. The current model was compared with the water depth measurements given by Puertas et al. (2004) (Fig. 13 a,b,c,d), for both designs and bed slopes and discharge of 65 l/s. As we can see the water depths predicted are quite similar with the measurements, with a slight difference at the area between the slots and the short baffles. There the numerical model predicts that the water depth increases sooner than it actually does.

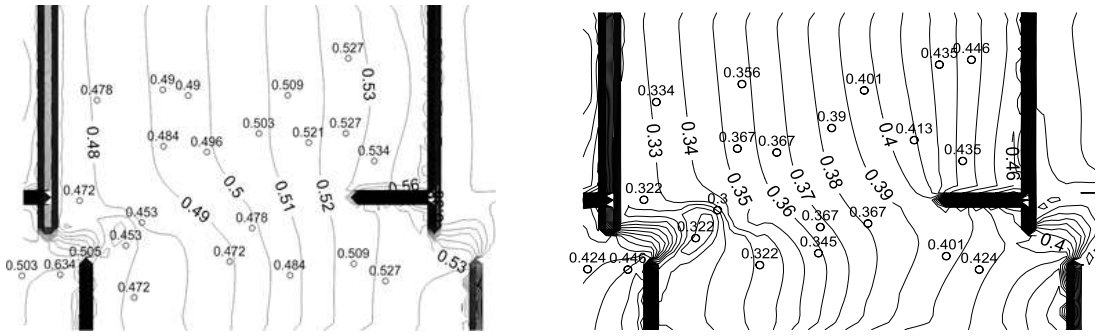

(a) T11 isolines

(b) T12 isolines

(c) T21 isolines

(d) T22 isolines

Figure 19 Contour lines of water-free surface.

(With the circle marks are depicted the measurements form Puertas et al.(2004))

From the measurements was concluded that the line that is perpendicular to the flow contour lines of design T1 create a 45 degree angle, with the straight line that connects the upstream and downstream slots, when at design T2 the contour lines are perpendicular to this line. This fact was partially proven from the numerical

model. At design T1 the perpendicular line is at 45 degrees near the slot, but this starts to change after the slot. For design T2 though we have a good prediction.

The maximum and minimum flow depths are also good predicted. The minimum occur just after the slot, that we observe a high water depth drop, and the maximum near the downstream baffle at the upper side of the vertical guiding element.
For design T2 the minimum water depth is also accurately predicted, after the slot, where we have a water level drop and the maximum close to the long downstream baffle near the outlet slot. All the results can be seen in table 1 above.

In the comparison of the measurements with the present model and the numerical model proposed by Cea et al.(2007) is obvious that both k-ε and RNG models give similar results. The k-ε predicts more accurately the water surface for the discharge of 105 l/s, while the RNG for 65 l/s with slight differences whatsoever. Furthermore the profile of the water surface longitudinal cut is better predicted by the RNG (Fig.14). Finally both underestimate the higher water depths near the downstream baffle.

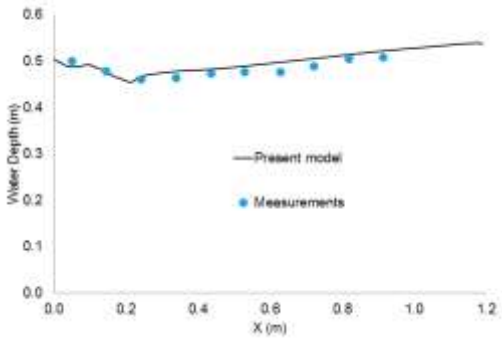

(a) T11 at section along the slot

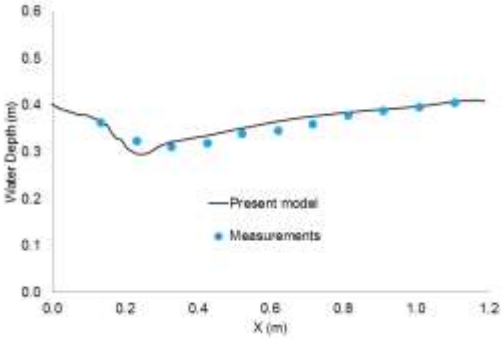

(b) T12 at section along the slot

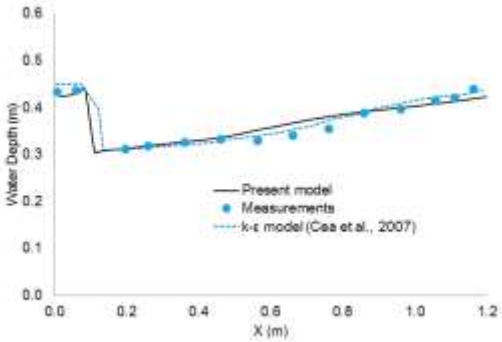

(c) T12 at section C16

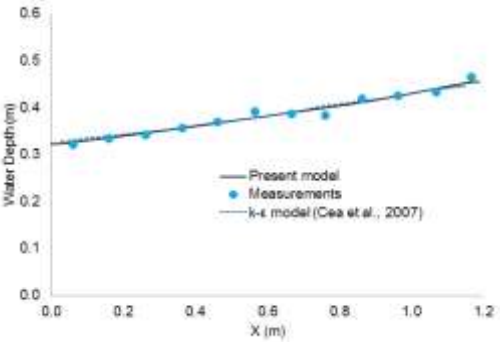

(d)T12 at section C76

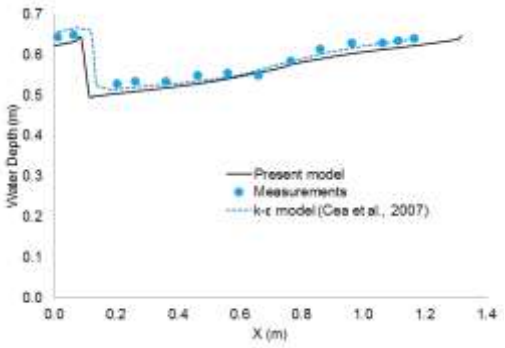

(e) T13 at section C16

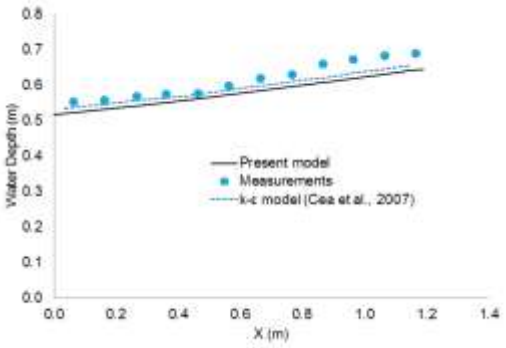

(f) T13 at section C76

Figure 20 Flow depths at various sections for pool design T1

Table 6. Statistic comparison of measurements with the models for the water depths for Scenarios of Design T1

	Water Depth									
	Scenario T11	Scenario T12					Scenario T13			
	Slot Region	C=16		Slot Region	C=76		C=16		C=76	
	Present Model	Present Model	k-ε Cea et al(2007)	Present Model	Present Model	k-ε Cea et al(2007)	Present Model	k-ε Cea et al(2007)	Present Model	k-ε Cea et al(2007)
Correration of Determination	0,793	0,933	0,976	0,879	0,965	0,965	0,967	0,969	0,976	0,954
MAPE	2,58%	2,59%	2,11%	2,83%	1,53%	1,65%	0,97%	1,79%	1,68%	3,82%
RMSE	0,014	0,013	0,009	0,013	0,008	0,008	0,008	0,011	0,014	0,029
Index of Agreement	0,878	0,976	0,991	0,965	0,990	0,989	0,991	0,986	0,975	0,885
Modified Index of Agreement	0,627	0,878	0,911	0,833	0,912	0,909	0,934	0,885	0,859	0,689

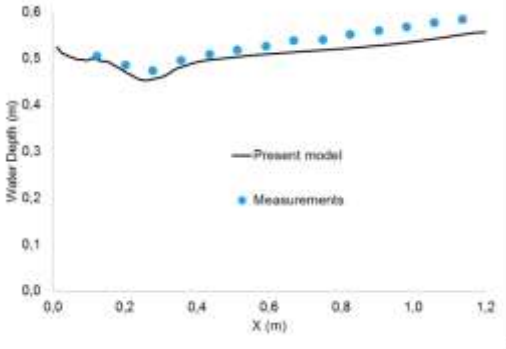

(a) T21 at section along the slot

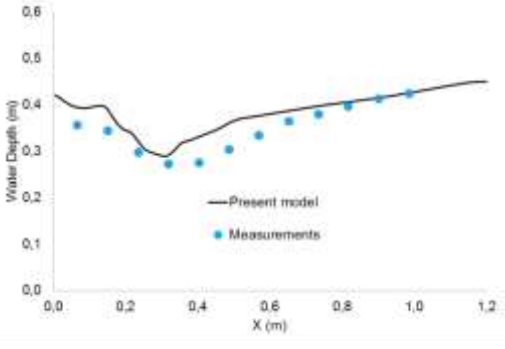

(b) T22 at section along the slot

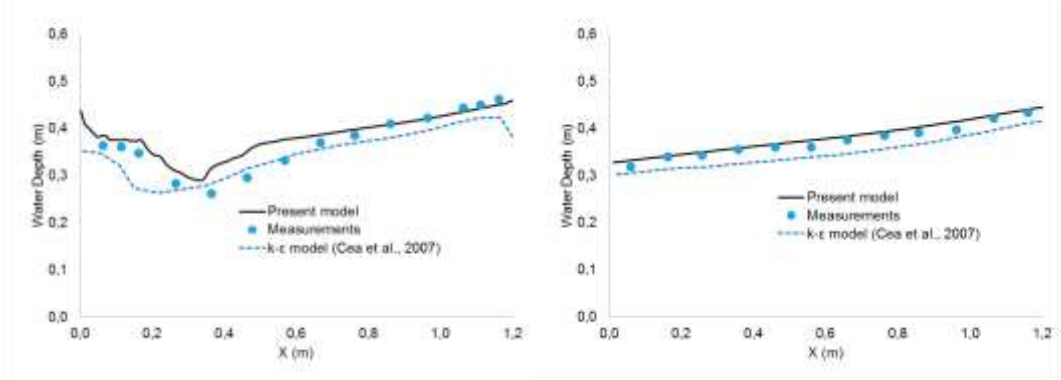

(c) T22 at section C14 (d)T22 at section C74

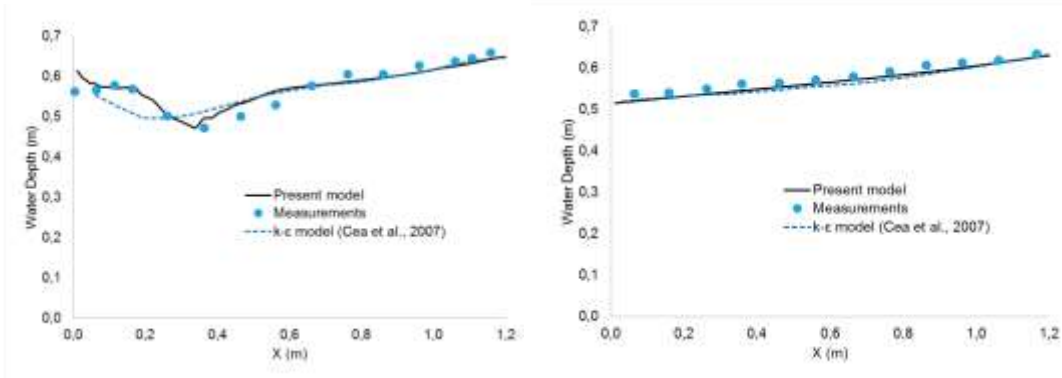

(e) T23 at section C14 (f)T23 at section C74

Figure 21 Flow depths at various sections for pool design T2

Table 7. Statistic comparison of measurements with the models for the water depths for Scenarios of Design T2

	Water Depth									
	Scenario T21	Scenario T22					Scenario T23			
	Slot Region	C=14		Slot Region	C=74		C=14		C=74	
	Present Model	Present Model	k-ε Cea et al(2007)	Present Model	Present Model	k-ε Cea et al(2007)	Present Model	k-ε Cea et al(2007)	Present Model	k-ε Cea et al(2007)
Correration of Determination	0,974	0,965	0,842	0,916	0,982	0,976	0,946	0,990	0,990	0,977
MAPE	4,140	5,556	7,331	7,696	2,396	6,487	2,596	6,878	2,025	2,595
RMSE	0,024	0,023	0,032	0,031	0,010	0,025	0,018	0,047	0,012	0,016
Index of Agreement	0,862	0,950	0,919	0,911	0,977	0,877	0,968	0,536	0,964	0,941
Modified Index of Agreement	0,602	0,775	0,720	0,731	0,841	0,617	0,816	0,322	0,794	0,744

Here also the statistics are in favor of the RNG k-epsilon turbulent model. Again all the correlations are described as strong, but the present model has the advantage of a 3D simulation, which shows better performance at the slot region. This indicates

that the slot region, which is of high importance for the fish, is mainly three dimensional, and the shallow water equations cannot predict the water depth accurately.

5.5 Turbulence Field

5.5.1 Kinetic energy and dissipation

Although the velocity fields are satisfactorily predicted, this usually does not occur to turbulence fields. This usually happens because of the nature of the closure models, which demands fine mesh to calculate the eddies created, which cost highly in computational time. Although it is not expected to have highly accurate results from the numerical models a comparison was made between the results of the present study, the results of Cea et al.(2007) and the results from the experimental measurements of Puertas et al. (2004). Because Puertas et al. (2004) were not able to measure the turbulent kinetic energy, they used the velocity data to produce it. The velocity time series were divided to two components the average and the turbulent. The turbulent component is the root mean square of the turbulent velocity fluctuations and it is equal to the standard deviation of the time series. Therefore the Turbulent kinetic energy was calculated as proposed by Rodi (1980) as :

$$k = \frac{u'^2 + v'^2 + w'^2}{2}$$

The results were quite satisfactory for both numerical models. The RNG gives slightly better predictions than the k-ε model for the turbulence field. The main difference is that the k-ε overestimates turbulence and RNG under estimates it slightly, but overall the high turbulence values that predicted are close to the experimental ones. In general the eddy viscosity models are not able to predict accurately the excessively high turbulence field and the strong swirl that is created, just after the inlet slot; therefore we can explain the inability to match exactly the experimental measurements (Fig.22,23 and 24).

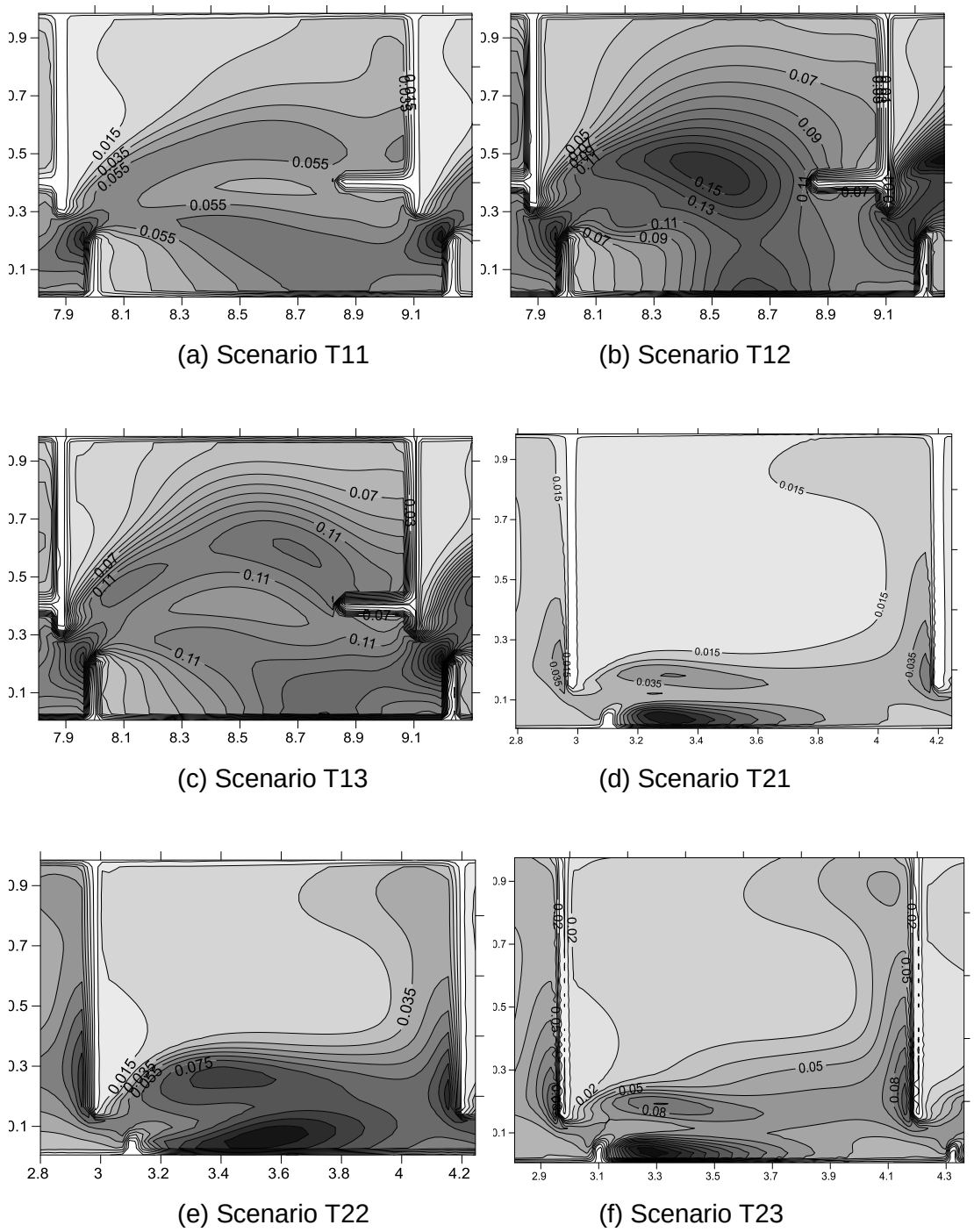

Figure 22 Turbulent Kinetic energy in J/Kg at the middle of the flow depth

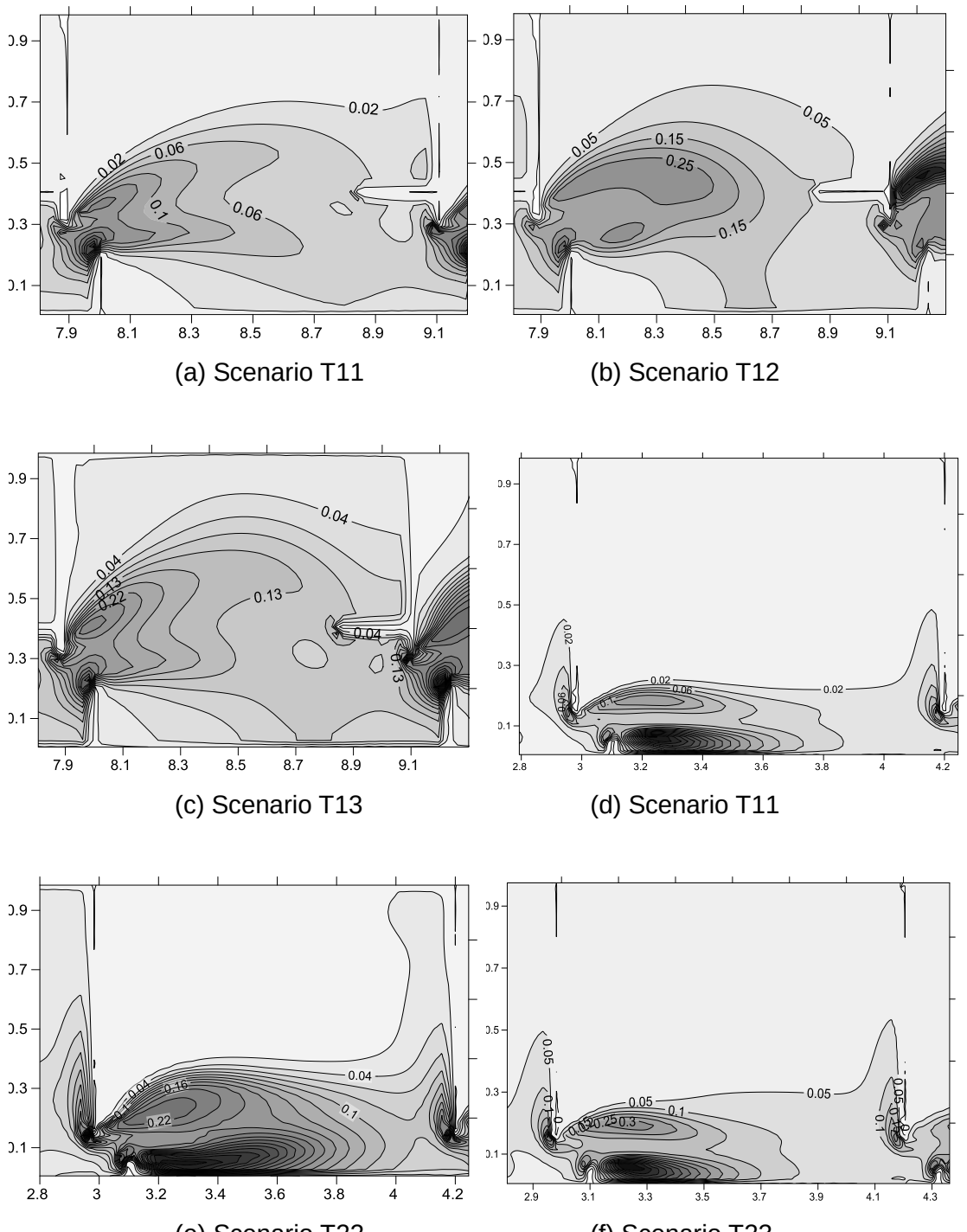

Figure 23 Turbulent dissipation in W/Kg at the middle of the flow depth

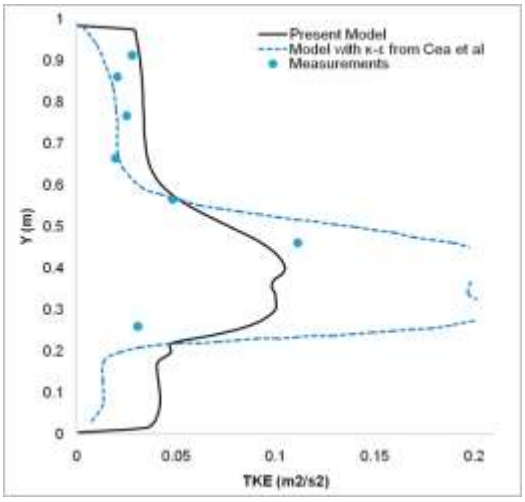

(a) T12 at section C16

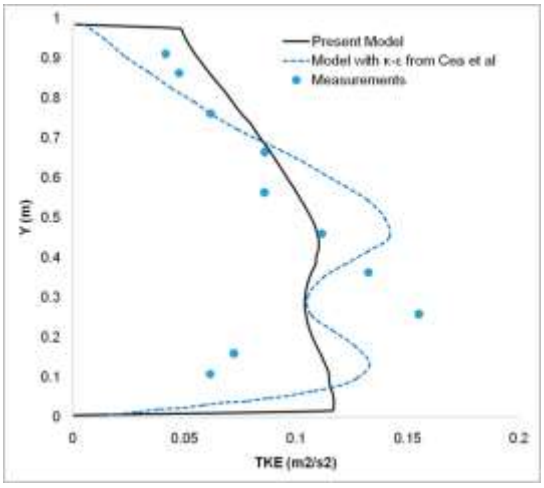

(b)T12 at section C86

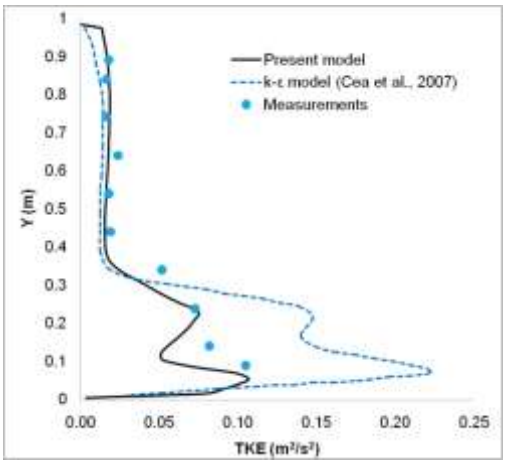

(c) T22 at section C26

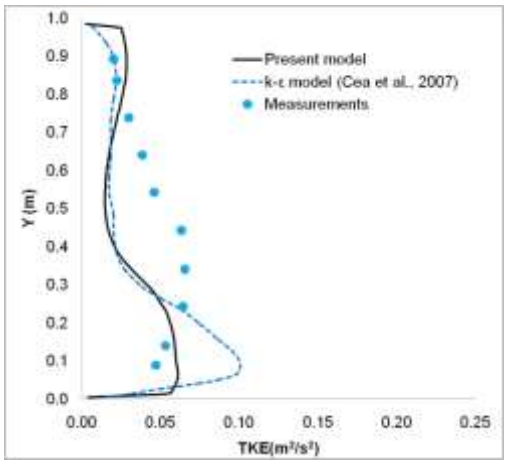

(d) T22 at section C86

Figure 24 Turbulent Kinetic energy for pool design T1 and T2 for various cross sections

Table 8. Statistic comparison of measurements with the models for the Turbulent Kinetic Energy for Scenarios T12 and T22

	Turbulent Kinetic Energy							
	Scenario T12				Scenario T22			
	C=16		C=86		C=26		C=86	
	Present Model	k-ε Cea et al(2007)	Present Model	k-ε Cea et al(2007)	Present Model	k-ε Cea et al(2007)	Present Model	k-ε Cea et al(2007)
Correration of Determination	0,552	0,763	0,373	0,324	0,878	0,918	0,084	0,112
MAPE	55,65%	64,43%	29,51%	39,08%	20,82%	53,30%	39,45%	47,09%
RMSE	0,023	0,044	0,029	0,037	0,017	0,047	0,023	0,030
Index of Agreement	0,818	0,785	0,725	0,740	0,907	0,801	0,548	0,529
Modified Index of Agreement	0,604	0,604	0,534	0,550	0,794	0,539	0,436	0,443

The statistics are again in favor of the present model, this time at both designs. This occurs probably because the RNG model is constantly calculating the some of the coefficients of the k-epsilon model, which considered being steady.

5.5.2 Reynolds stresses

Reynolds stresses are the values of the Reynolds stress tensor in the Reynolds Averaged Navier Stokes equations. These are the unknown variables that need an equation in order to solve the RANS equations. Boussinesque proposed his hypothesis that as the shear stresses of Navier Stokes equations have the dynamic viscosity v that is a characteristic of the fluid, the turbulent field has also a coefficient in front of the Reynolds stresses, which he called eddy viscosity vt. In the recirculation field the hypothesis is written as

$$\overline{-u_i' u_j'} = -\frac{2}{3} k \delta_{ij} + v_t \left(\frac{\partial \overline{u_i}}{\partial x_j} + \frac{\partial \overline{u_j}}{\partial x_i}\right) \quad \text{(Eq.15)}$$

Eddy viscosity is not a characteristic of the fluid, but is changing constantly with the flow. Based on the Boussinesque hypothesis lots of turbulent models have been created, including the k-epsilon family of turbulent closure models. When the turbulent field is homogenous and isotropic, as the k-epsilon suggests, the normal stresses are equal. This is something that was not proven in experiments, were the second part of Eq. 15 is not equal to zero.

Since FLOW – 3D does not calculate the Reynolds stresses, they were calculated in order to be compared with the measurements and the k-epsilon model from Eq. 15 as proposed by Launder et al., (1975).

The results show that the RNG model fits better in the measurements in comparison to the standard k-epsilon model, and that the three dimensional model is performing better than the 2D shallow water model in the area of the slot, which is of grave importance to the fish.

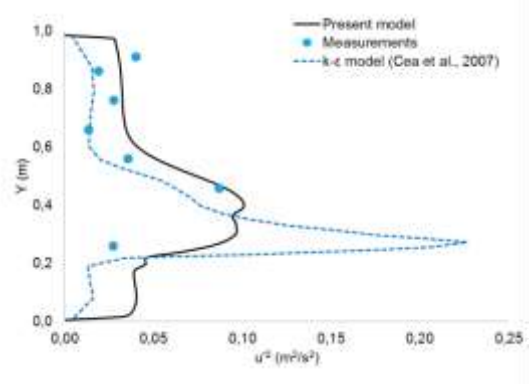

(a) u'^2 for T12 at section C16

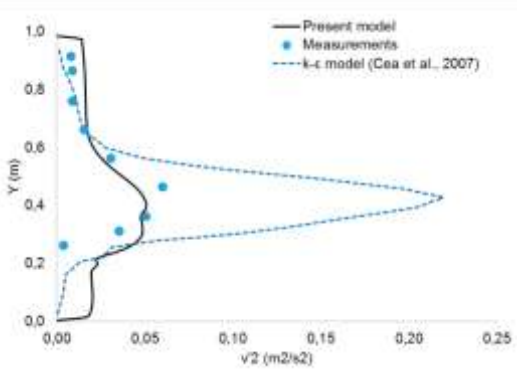

(b) v'^2 for T12 at section C16

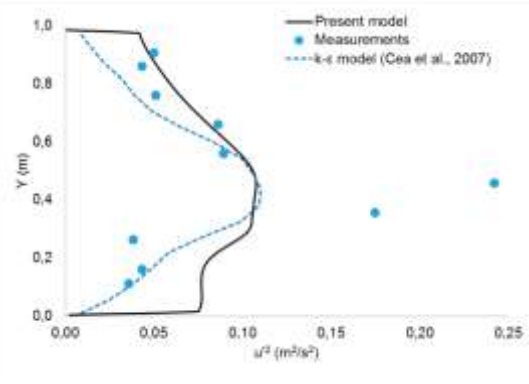

(c) u'^2 for T12 at section C46

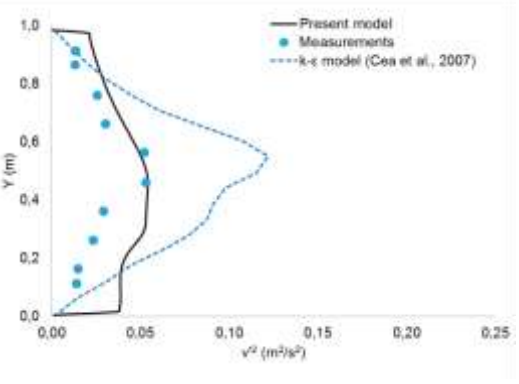

(d) v'^2 for T12 at section C46

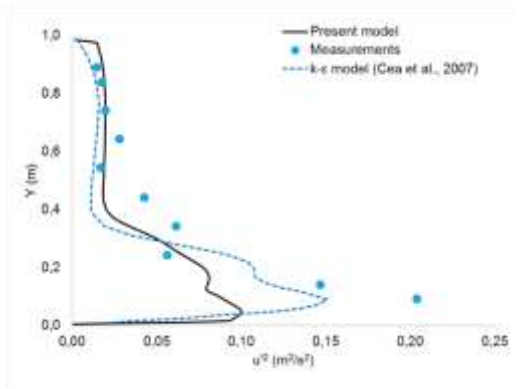

(e) u'^2 for T22 at section C46

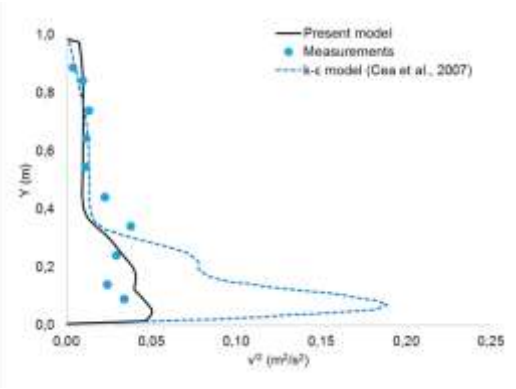

(f) v'^2 for T22 at section C46

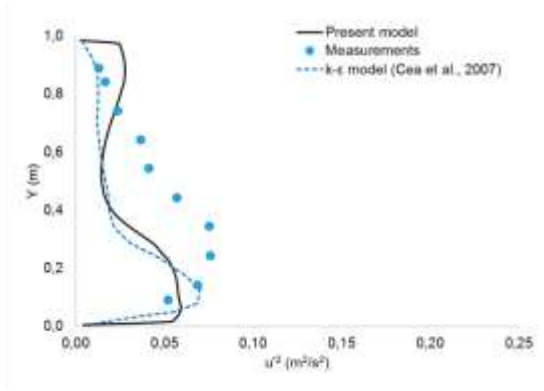

(g) u'^2 for T22 at section C86

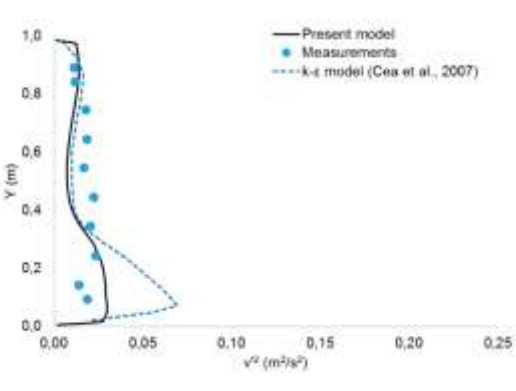

(h) v'^2 for T22 at section C86

Figure 25 Normal Reynolds Stresses at various cross sections

Table 9. Statistic Indexes for Normal Reynolds Stresses at Design T1

	Scenario T12 - Normal Reynolds Stresses							
	C=16				C=46			
	U'^2		V'2		U'^2		V'2	
	Present Model	k-ε Cea et al(2007)	Present Model	k-ε Cea et al(2007)	Present Model	k-ε Cea et al(2007)	Present Model	k-ε Cea et al(2007)
Correration of Determination	0,456	0,005	0,855	0,446	0,362	0,149	0,368	0,051
MAPE	72,45%	125,52%	92,53%	83,13%	50,98%	37,39%	77,19%	122,57%
RMSE	0,024	0,071	0,595	0,580	0,054	0,051	0,017	0,041
Index of Agreement	0,749	0,210	0,375	0,357	0,566	0,716	0,670	0,538
Modified Index of Agreement	0,497	0,353	0,270	0,283	0,447	0,599	0,453	0,309

Table 10. Statistic Indexes for Normal Reynolds Stresses at Design T2

	Scenario T22 - Normal Reynolds Stresses							
	C=46				C=86			
	U'^2		V'2		U'^2		V'2	
	Present Model	k-ε Cea et al(2007)	Present Model	k-ε Cea et al(2007)	Present Model	k-ε Cea et al(2007)	Present Model	k-ε Cea et al(2007)
Correration of Determination	0,841	0,850	0,462	0,380	0,243	0,352	0,000	0,001
MAPE	29,58%	38,90%	43,08%	113,68%	53,93%	43,71%	45,12%	89,00%
RMSE	0,044	0,028	0,010	0,055	0,024	0,026	0,009	0,022
Index of Agreement	0,760	0,934	0,808	0,330	0,632	0,694	0,510	0,609
Modified Index of Agreement	0,673	0,771	0,653	0,322	0,484	0,551	0,395	0,494

From statics we can confirm what it is obvious from the graphs at Fig. 25. The Reynolds stresses calculated from the present model show better correlation to the measurements, almost with every index used. That is probably also the advantage of the 3D model over the 2D one.

Chapter 6. Conclusions

In the present study we created a 3-D CFD model in the FLOW - 3D software, and we performed calculations using the Finite Volume Method to solve the Reynolds Averaged Navier Stokes equations. The closure turbulent model was the Renormalised Group k-epsilon.

The model was based on an experimental model created from Puertas et al.(2004) based on the designs proposed by Rajaratnam et al. (1992). The results were compared with the results from the experiment above and the work of Cea et al.(2007) using graphs and statistical indexes.

The results showed that the model was able to predict the flow field satisfactorily, since the results found to be close to the measurements. The shallow water equations give similar results to a three-dimensional model, with small differences near the slot regions. Furthermore the three-dimensional model produces better velocity profiles, especially to higher discharges.

The RNG can predict a slightly more accurate turbulence field as shown from the comparison through the statistical indexes. The k-ε model overestimates the turbulent kinetic energy, due to the constants it uses, and the difficulties of predicting flows of high swirl.

The flow depth is also satisfactorily predicted by the present model, as shown from the depth graphs, but also is able to be satisfactorily accurate at the slot region where we have a drop of the flow depth, something that the k-epsilon model with shallow water equations was not able to predict. Both models overestimate the flow depth near the right side wall and to the downstream baffle.

The general conclusion would be that the numerical models can provide guidelines at the design of new fish-passes, but we did not have solid results to support that the design can rely only to numerical models and predictions that are made from the solution of the RANS equations.

Chapter 7. References

1. Flow Science Inc. FLOW-3D User's Manual, Flow Science Inc, 2014.

2. Abdelaziz S.M.A. (2013). Numerical simulation of fish behavior and fish movement through passages, Ph.D. Thesis, Technische Universität München.

3. Alvarez-Vázquez, L.J., A. Martínez, et al. (2007). Vertical slot fishways: Mathematical modeling and optimal management. Journal of Computational and Applied Mathematics 218(2): 395-403.

4. Alvarez-Vázquez, L., Martínez, A., Vázquez-Méndez, M., & Vilar, M. (2008). An optimal shape problem related to the realistic design of river fishways. Ecological Engineering, 32(4), 293-300. doi:10.1016/j.ecoleng.2007.10.008

5. Arrowsmith, C. S., & Zhu, Y. (2014). Comparison between 2D and 3D hydraulic modelling approaches for simulation of vertical slot fishways. Hydraulic Structures and Society - Engineering Challenges and Extremes. doi:10.14264/uql.2014.49

6. Barton, A. F., & Keller, R. J. (2003). 3D Free Surface Model for a Vertical Slot Fishway. Clayton, Victoria, Australia.

7. Bombač, M., Novak, G., Rodič, P., & Četina, M. (2014). Numerical and physical model study of a vertical slot fishway. Journal of Hydrology and Hydromechanics, 62(2). doi:10.2478/johh-2014-0013

8. Bousmar, D., Li, Z., Baugnee, A., & Degreef, J.-C. (2015, June 28). Flow Pattern in Fish-passes: Comparison of Numerical Models. 4. Hague, Netherlands: E- Proceedings of the 36th IAHR World Congress.

9. Cea, L., Pena, L., Puertas, J., Vázquez-Cendón, M. E., & Peña, E. (2007). Application of Several Depth-Averaged Turbulence Models to Simulate Flow in Vertical Slot Fishways. Journal of Hydraulic Engineering, 133(2), 160-172. doi:10.1061/(asce)0733-9429(2007)133:2(160)

10. Chorda, J., Maubourguet, M. M., Roux, H., Larinier, M., Tarrade, L., & David, L. (2010). Two-dimensional free surface flow numerical model for vertical slot fishways. Journal of Hydraulic Research, 48(2), 141-151. doi:10.1080/00221681003703956

11. Fujihara, M., Fukushima, T., & Tachibana, K. (2002). Numerical Modelling Of Flows In Vertical Single-Slot And Double-Slot Fishways. Advances in Hydraulics and Water Engineering. doi:10.1142/9789812776969_0188

12. Heimerl, S., Hagmeyer, M., & Echteler, C. (2008). Numerical flow simulation of pool-type fishways: New ways with well-known tools. Hydrobiologia, 609(1), 189-196. doi:10.1007/s10750-008-9413-1

13. Hirt, C., & Nichols, B. (1981). Volume of fluid (VOF) method for the dynamics of free boundaries. Journal of Computational Physics, 39(1), 201-225. doi:10.1016/0021-9991(81)90145-5

14. Katopodis, C., Kells, J., & Acharya, M. (2001). Nature-Like and Conventional Fishways: Alternative Concepts? Canadian Water Resources Journal, 26(2), 211-232. doi:10.4296/cwrj2602211

15. Katopodis, C., & Williams, J. G. (2012). The development of fish-passage research in a historical context. Ecological Engineering, 48, 8-18. doi:10.1016/j.ecoleng.2011.07.004

16. Khan, L. A. (2006). A Three-Dimensional Computational Fluid Dynamics (CFD) Model Analysis of Free Surface Hydrodynamics and Fish-passage Energetics in a Vertical-Slot Fishway. North American Journal of Fisheries Management, 26(2), 255-267. doi:10.1577/m05-014.1

17. Klein, J.,Oertel, M., (2015). Comparison of between crossbar block ramp and Vertical Slot Fish-pass via Numerical 3D CFD Simulation. Hague, Netherlands: E- Proceedings of the 36th IAHR World Congress.

18. Larinier, M., Porcher, J. P., Travade, F., and Gosset, C. 19981. Passes a Poissons. Expertise conception des ouvrages de franchissement, Collection Mise Au Point Conseil Superior de la Péache, Paris.

19. Launder, B. E., Reece, G. J., & Rodi, W. (1975). Progress in the development of a Reynolds-stress turbulence closure. Journal of Fluid Mechanics, 68(03), 537. doi:10.1017/s0022112075001814

20. Liu, M., Rajaratnam, N., & Zhu, D. Z. (2006). Mean Flow and Turbulence Structure in Vertical Slot Fishways. Journal of Hydraulic Engineering, 132(8), 765-777. doi:10.1061/(asce)0733-9429(2006)132:8(765)

21. Marriner, B. A., Baki, A. B., Zhu, D. Z., Thiem, J. D., Cooke, S. J., & Katopodis, C. (2014). Field and numerical assessment of turning pool hydraulics in a vertical slot fishway. Ecological Engineering, 63, 88-101. doi:10.1016/j.ecoleng.2013.12.010

22. Puertas, J., Pena, L., & Teijeiro, T. (2004). Experimental Approach to the Hydraulics of Vertical Slot Fishways. Journal of Hydraulic Engineering, 130(1), 10-23. doi:10.1061/(asce)0733-9429(2004)130:1(10)

23. Rajaratnam, N., Katopodis, C., & Solanki, S. (1992). New designs for vertical slot fishways. Canadian Journal of Civil Engineering, 19(3), 402-414. doi:10.1139/l92-049

24. Rajaratnam, N., Vinne, G. V., & Katopodis, C. (1986). Hydraulics of Vertical Slot Fishways. Journal of Hydraulic Engineering, 112(10), 909-927. doi:10.1061/(asce)0733-9429(1986)112:10(909)

25. Stamou A. (2015). Ecological Modelling of Surface Waters, Lecture Notes, TUM.

26. Stamou A., Economou A., Kartsakali A. and Papadonikolaki G. (2015), Fish-passes in small hydroelectric plants: their current empirical design and the future using integrated mathematical models, 3rd Joint Conference:13th of Greek Hydrotechnic Union, 9th of Greek Committee for Water Resources Management, 1st of Hellenic Water Association of “Integrated Management of Water Resources in New Era”, 10-12 December 2015, Athens, Greece.

27. Puzdrowska, M. S. (2013.). Application of numerical methods in the design and analysis of fish-pass efficiency. Retrieved October 05, 2016, from http://pwr-wroc.academia.edu/MartaSimkowskaPuzdrowska

28. Rodi, W. (1980) Turbulence models and their applications in hydraulics—A state-of-the-art review, The Netherlands International Association of Hydraulic Research, Delft, The Netherlands.

29. Tarrade, L., Pineau, G., Calluaud, D., Texier, A., David, L., & Larinier, M. (2010). Detailed experimental study of hydrodynamic turbulent flows generated in vertical slot fishways. Environmental Fluid Mechanics, 11(1), 1-21. doi:10.1007/s10652-010-9198-4

30. Tarrade L., Texier A., David L., Pineau G. and Larinier M., 2006. An experimental study of turbulent flow in vertical slot fishways. 12th International Symposium on Flow Visualization, German Aerospace Center (DLR), Göttingen, 12 p.

31. Versteeg, H. K., & Malalasekera, W. (1995). An introduction to computational fluid dynamics: The finite volume method. Harlow, Essex, England: New York.

32. Wang, R., David, L., & Larinier, M. (2010). Contribution of experimental fluid mechanics to the design of vertical slot fish-passes. Knowledge and Management of Aquatic Ecosystems, (396), 02. doi:10.1051/kmae/2010002

33. Wu, S., Rajaratnam, N., & Katopodis, C. (1999). Structure of Flow in Vertical Slot Fishway. Journal of Hydraulic Engineering, 125(4), 351-360. doi:10.1061/(asce)0733-9429(1999)125:4(351)

34. Yakhot, V., & Orszag, S. A. (1986). Renormalization group analysis of turbulence. I. Basic theory. Journal of Scientific Computing, 1(1), 3-51. doi:10.1007/bf01061452